

An Outer Arm in the Second Galactic Quadrant: Structure

Xinyu Du^{1,2,3}, Ye Xu^{1,3}, Ji Yang^{1,3}, Yan Sun^{1,2,3}, Facheng Li^{1,2,3}, Shaobo Zhang^{1,3},
Xin Zhou^{1,3}

xydu@pmo.ac.cn; xuye@pmo.ac.cn

ABSTRACT

The lack of arm tracers, especially the remote tracers, is one of the most difficult problems preventing us from studying the structure of the Milky Way. Fortunately, with its high-sensitivity CO survey, the Milky Way Imaging Scroll Painting (MWISP) project offers such an opportunity. Since completing about one third of its mission, an area of $l = [100, 150]^\circ$, $b = [-3, 5]^\circ$ has nearly been covered. The Outer arm of the Milky Way first clearly revealed its shape in the second galactic quadrant in the form of molecular gas — this is the first time that the Outer arm has been reported in such a large-scale mapping of molecular gas. Using the 115 GHz $^{12}\text{CO}(1-0)$ data of MWISP at the LSR velocity $\simeq [-100, -60]$ km s⁻¹ and in the area mentioned above, we have detected 481 molecular clouds in total, and among them 332 (about 69%) are newly detected and 457 probably belong to the Outer arm. The total mass of the detected Outer arm clouds is $\sim 3.1 \times 10^6 M_\odot$. Assuming that the spiral arm is a logarithmic spiral, the pitch angle is fitted as $\sim 13.1^\circ$. Besides combining both the CO data from MWISP and the 21 cm HI data from the Canadian Galactic Plane Survey (CGPS), the gas distribution, warp, and thickness of the Outer arm are also studied.

Subject headings: catalogs – Galaxy: structure – ISM: molecules – ISM: clouds

1. Introduction

It is well-known that our galaxy has a spiral structure, (Oort et al. 1958; Bok 1959) but a detailed understanding of the Milky Way is still lacking. Since Georgelin & Georgelin

¹Purple Mountain Observatory, Chinese Academy of Science, Nanjing 210008, China

²Graduate University of the Chinese Academy of Sciences, 19A Yuquan Road, Shijingshan District, Beijing 100049, China

³Key Laboratory of Radio Astronomy, Chinese Academy of Science, Nanjing 210008, China

(1976) presented a large-scale spiral pattern with HII regions, nearly 100 Milky Way models have been proposed (Steiman-Cameron 2010). However, most models share the same large structure in spite of differing details (e.g., Russeil et al. 2007; Vallée 2008; Hou & Han 2014).

The fact that there exists a spiral arm beyond the Perseus arm has been generally recognized for a long time. Since Moffat & Vogt (1975) noticed that several young star clusters were located far beyond the position of the Perseus arm, more work has been done to confirm the existence of this external arm. Henderson et al. (1982) first systematically studied the distribution of HI in the outer galaxy beyond the solar circle, which is a vast frontier of our galaxy. Heyer et al. (1998) described the molecular image of outer galaxy with FCRAO CO survey results, providing the evidence for the presence of molecular clouds in this outer area. Negueruela & Marco (2003) traced the external arm using OB stars and concluded that the Cam OB3 association lies on it. On the basis of maser source (associated with high-mass star-forming region, HMSFR) distances, Reid et al. (2014) first delineated several spiral arms, including the Outer arm, using the trigonometric parallax method. In addition, detailed parallax results and analyses of the Outer arm are also presented by Hachisuka et al. (2015)

However, the accurate maser source positions cannot outline the distributions of interstellar gases. The FCRAO CO survey only traced the high-mass molecular clouds because of its poor sensitivity. Fortunately, the Milky Way Imaging Scroll Painting (MWISP) project ¹ provides such a chance to study the molecular gases with the no-bias high sensitive $^{12}\text{CO}(1-0)$, $^{13}\text{CO}(1-0)$ and $\text{C}^{18}\text{O}(1-0)$ observations. Due to such high-sensitive observations, a new spiral arm (hereafter the New arm) beyond the Outer arm has been discovered by Sun et al. (2015). Combining the $^{12}\text{CO}(1-0)$ observations of MWISP and atomic hydrogen data from the Canadian Galactic Plane Survey (CGPS; Taylor et al. 2003), we presented the results of the Outer arm: the arm located between the Perseus arm and the New arm. The results derived from $^{13}\text{CO}(1-0)$ and $\text{C}^{18}\text{O}(1-0)$ data and further analyses will be published in our future works.

Please note that the Outer arm does not have a particular name yet. Some authors have labeled it as the “Cygnus arm”, or the “Perseus +I arm”, or the “Norma—Cygnus arm” (Vallée 2008). Otherwise, the name “Outer arm” is also widely used (e.g., Dame et al. 2001; Reid et al. 2014). Considering the fact that the name “Cygnus” has been described as the location near the Sun in some early papers, here we choose the name “Outer arm” in this paper to avoid confusion.

In Sect. 2 we introduce our CO observation conditions and archival data of atomic

¹<http://english.dlh.pmo.cas.cn/ic/> or <http://www.radioast.nsd.cas.cn/mwisp.php>

hydrogen. In Sect. 3 we describe how we pick out the Outer arm clouds and briefly study their properties. In Sect. 4 we study the properties of the Outer arm, including the pitch angle, the gas distribution, the thickness, and the warp. The summary is given in Sect. 5.

2. Observations and archival data

2.1. CO observations

The ^{12}CO (1 – 0), ^{13}CO (1 – 0) and C^{18}O (1 – 0) lines were observed simultaneously using the Purple Mountain Observatory Delingha (PMODLH) 13.7 m telescope from 2011 September to 2015 March as one of the scientific demonstration regions for the MWISP project, which is the first no-bias high-sensitivity CO survey with such a large-scale aiming at $l = [-10, 250]^\circ$, $b = [-5, 5]^\circ$. With the on-the-fly (OTF) observing mode, MWISP now has completed about one-third of its plan, and an area of $l = [100, 150]^\circ$, $b = [-3, 5]^\circ$ has mostly been covered—the total area was 288 square degrees. A superconductor-insulator-superconductor (SIS) superconducting receiver with a nine-beam array was used as the front end (Shan et al. 2012). A Fast Fourier Transform (FFT) spectrometer with a total bandwidth of 1000 MHz and 16,384 channels was used as the back end. For the 115 GHz ^{12}CO (1 – 0) observations, the main beam width was about $52''$, the main beam efficiency (η_{MB}) was 0.46, and the typical rms noise level was ~ 0.5 K, corresponding to a channel width of 0.16 km s $^{-1}$. (~ 0.2 K per 0.8 km s $^{-1}$ channel, which is 3 times better than the FCRAO OGS sensitivity.) All the data were corrected by $T_{\text{MB}} = T_{\text{A}}^*/\eta_{\text{MB}}$. The data were sampled every $30''$. All the data were reduced using the GILDAS/CLASS package.

2.2. Archival data of atomic hydrogen

The 21 cm line data were retrieved from the CGPS. We downloaded data of $l = [63, 155]^\circ$, $b = [-3, 5]^\circ$ from the Canadian Astronomy Data Centre². The velocity coverage of the data is in the range of -153 to 40 km s $^{-1}$, with a channel separation of 0.82 km s $^{-1}$. The survey has a spatial resolution of $58''$, which is comparable to our CO observations.

²<http://cadc.hia.nrc.ca>

3. Analysis of clouds

We have detected 481 clouds in total; 332 (about 69%) clouds are newly detected, 457 clouds are identified in the Outer arm, and 24 are identified in the New arm. Among the Outer arm clouds, 7 are reported by Brand & Wouterloot (1994) (hereafter BW94), 75 are reported by Heyer et al. (2001) (hereafter HCS01 clouds), 125 are reported by Brunt et al. (2003) (hereafter BKP03). And all 24 of the New arm clouds are newly detected. (These 24 New arm clouds do not overlap with the clouds detected by Sun et al. 2015.) The parameters of all the 481 clouds are summarized in Table.1.

3.1. Cloud identification

Because of the differential rotation of the Milky Way, most LSR velocities that are consistent with circular Galactic rotation are negative in the second quadrant. Starting from $V_{\text{LSR}} \sim 0 \text{ km s}^{-1}$, increasingly negative velocities successively trace the Local arm, the Perseus arm, the Outer arm, and the New arm. In order to find all of the Outer arm clouds, we need to know the Outer arm LSR velocity range at every galactic longitude. As mentioned above, the Outer arm LSR velocity is located between the Perseus arm and the New arm, which provides us with a clue for picking out the clouds. First, using the HI data from the CGPS, we plotted the longitude-velocity map of HI, integrated over all latitudes (from -3° to 5°). Second, we projected the spatial (x, y) curves of the Outer arm, the Perseus arm (both fitted by Reid et al. 2014, and hereafter the Reid Outer spiral and the Reid Perseus spiral), and the New arm (fitted by Sun et al. 2015, and hereafter the Sun New spiral) on that HI longitude-velocity map. (In other words, we converted the dashed curves shown in Fig. 3 into the ones shown in Fig. 5. And the converting method is presented in detail in Sect. 4.3.) And then we marked all the HCS01 clouds on that map. Combining the HI map, the positions of the longitude-velocity curves, and HCS01 clouds, we can estimate the velocity range of the Outer arm as a function of galactic longitude. Third, we compiled an automatic procedure to list all the positions with emissions greater than 2.5σ of the data cube at that velocity range (where σ is the typical rms noise and $= 0.5 \text{ K}$). Last, we checked both the list and data cube and identified the clouds via the naked eye. It is necessary to emphasize that we did not separate the isolated clouds or cloud complexes into small pieces of molecular clumps. In other words, some of the clouds have multiple spectral or spatial peaks.

Finally, we have detected 481 clouds in total. But not all of them belong to the Outer arm. Of these clouds, 24 clouds may be located in the New arm, since the velocity gap between the 24 clouds and the other ones is relatively large in the zoomed-in longitude-

velocity map.

However, it is necessary to point out that the Outer arm clouds that we found do not absolutely belong to that arm. From $l \simeq 100^\circ$ to 120° , there exists an arm-blending region. The LSR velocities of HI gas of the Perseus arm and the Outer arm are mixed together (see Fig. 5 and 6). Also, the LSR velocity gap of CO between the two arms is not obvious. Since our cloud identification criterion is based on the LSR velocity, it is difficult to pick out Outer arm clouds in that region. We may omit some clouds with an LSR velocity $\gtrsim -70 \text{ km s}^{-1}$, or falsely pick the clouds that may be located at the inter-arm area.

3.2. Cloud parameters

Heliocentric distance is one of the most important values for studying both the cloud properties and the spiral structure. Generally there are three methods for measuring the distance: trigonometric parallax, photometry, and kinematic method. And the accuracy of the trigonometric parallax and photometry methods is better than that of the kinematic method. (see Xu et al. 2006) However, there is only one source with a parallax distance and a luminosity distance in the Outer arm region: the one associated with MWISP G135.267+02.800 —its parallax distance is 6.0 kpc (Reid et al. 2014) and its luminosity distance is also 6.0 kpc (Hou & Han 2014). So the kinematic method is the only choice for us.

We chose to use the kinematic distances on the basis of the galactic parameters of Model A5 of Reid et al. (2014) ($\Theta_0 = 240 \text{ km s}^{-1}$, $R_0 = 8.34 \text{ kpc}$, $\frac{d\Theta}{dR} = -0.2 \text{ km s}^{-1} \text{ kpc}^{-1}$, $U_\odot = 10.7 \text{ km s}^{-1}$, $V_\odot = 15.6 \text{ km s}^{-1}$, $W_\odot = 8.9 \text{ km s}^{-1}$, $\bar{U}_s = 2.9 \text{ km s}^{-1}$, $\bar{V}_s = -1.6 \text{ km s}^{-1}$, hereafter Reid model) and the FORTRAN source code provided by Reid et al. (2009). Note that all of the cloud distances we finally used are kinematic distances, including MWISP G135.267+02.800.

The Reid model is much better than the IAU model (namely $\Theta_0 = 220 \text{ km s}^{-1}$, $R_0 = 8.5 \text{ kpc}$). Take the cloud MWISP G135.267+02.800 as an example. Its parallax and luminosity distances both are 6.0 kpc, the Reid kinematic distance (using Reid model) is 6.7 kpc, whereas the IAU kinematic distance (using IAU model) is 8.6 kpc. A detailed comparison can be seen in the Section 4 of Reid et al. (2009)

However, one should also keep in mind that there still exist the biases from the assumption of circular motion inherent in this kinematic distance model. In the second galactic quadrant the kinematic distance may be a little larger than the real distance, just as seen in the example of MWISP G135.267+02.800 or the left panel of Fig. 3. A detailed discussion about the biases is presented in Sect. 4.2.

Knowing the distance d and latitude b we calculated the scale height Z by $Z = d \sin(b)$. And using b , Z , d and longitude l , we calculated the galactocentric radius R with $R^2 = d^2 \cos^2(b) + R_0^2 - 2R_0d \cos(b) \cos(l) + Z^2$.

The cloud solid angle A is defined by the 3σ limits. The cloud diameter D is obtained after the beam deconvolution: $D = d\sqrt{\frac{4}{\pi}A - \theta_{\text{MB}}^2}$ (Ladd et al. 1994), where θ_{MB} is the main beam width. Adopting the CO-to-H₂ X factor $1.8 \times 10^{20} \text{cm}^{-2} (\text{K} \cdot \text{km s}^{-1})^{-1}$ (Dame et al. 2001), cloud mass is calculated from $M = 2\mu m_{\text{H}} X \pi (\frac{D}{2})^2 \int T_{\text{B}} dV$, where $\mu = 1.36$ (Hildebrand 1983) is the mean atomic weight per H atom in the ISM, m_{H} is the H atomic mass, and $\int T_{\text{B}} dV$ is the integrated intensity of the T_{peak} spectrum. However, the mass is probably underestimated since the X factor adopted is measured in the solar neighborhood, and a recent study has suggested an increase of X in the outer Galaxy. (Abdo et al. 2010)

3.3. Comparison with HCS01

Heyer et al. (2001) have used the CO data of the FCRAO Outer Galaxy Survey to identify molecular clouds. To make a comparison, we plotted the distributions of line width, size, and mass for the HCS01 Outer arm clouds and ours. We have two reasons for not comparing the clouds with BW94 and BKP03: (i) the number of BW94 clouds is too few (ii) the BKP03 clouds are generated by the same data but from a different method than the HCS01 clouds, and their method tends to find out small-size molecular clumps, which is not consistent with our cloud identification criterion. Fig.1 shows the results. One may notice that there are 102 clouds of HCS01 in Fig. 1, but only 75 clouds are labeled in Table. 1. The reason is the different cloud identification methods: HCS01 includes both small, isolated clouds and clumps within larger cloud complexes, but our catalog only includes isolated clouds and cloud complexes. So the clouds are not exactly matched one-to-one.

Since the cloud heliocentric distances of HCS01 are derived from the IAU model, the sizes and masses are correspondingly biased. In order to make our comparison using the same criterion, we revised the distances of the Reid model and the sizes and masses are correspondingly revised.

However, the comparison result is against expectations. The signal-to-noise ratio of our data is higher than that of HCS01. Consequently, HCS01 should have contained more luminous (and therefore more massive) clouds. But the distribution shows that the fractions of small sizes and low masses of HCS01 are higher than those of ours. Two main reasons may have caused this: (i) HCS01 includes smaller clumps within larger cloud complexes, but we did not detach clumps from cloud complexes. (ii) Because of our higher signal-to-noise

ratio, we can detect a larger angle area for the same cloud, which results in larger sizes and masses.

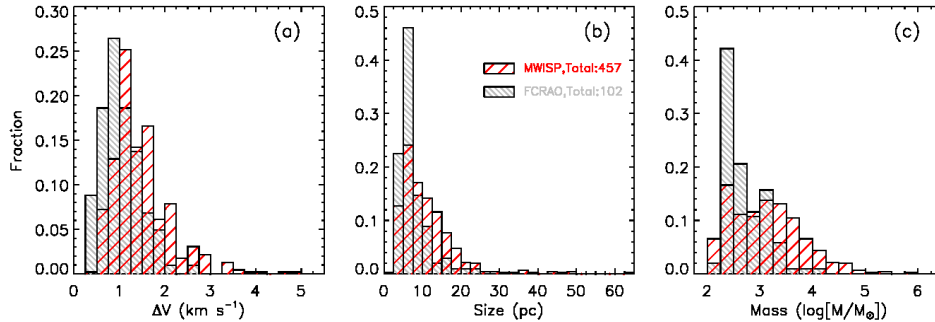


Fig. 1.— Distribution of the Outer arm cloud line width (a), size (b), and mass (c). The red and gray shades indicate the results from MWISP and FCRAO respectively.

4. Properties of Outer arm

4.1. Pitch angle

Spiral arms of external galaxies are usually approximated by logarithmic spirals. This is a simple but reasonable assumption and is also applicable to our Milky Way galaxy. That the pitch angle of one spiral is constant is one of the properties of a logarithmic spiral. Usually, the spiral arms of one galaxy are roughly fitted by logarithmic spirals with the same pitch (e.g., Vallée 2008), or more accurately, different spiral arms are fitted by different pitches (e.g., Russeil 2003). And sometimes even one spiral arm is fitted by varying the pitch angle (e.g., the Sagittarius arm in Taylor & Cordes 1993). In fact, Honig & Reid (2015) recently showed that in some external galaxies, the pitch angle in the same spiral arm varies, and the variance is as large as that among different arms within the same galaxy. So a more accurate assumption may be that the pitch angle of one segment of the arm within one galaxy is constant.

Now we assume that the segment from $l = 100^\circ$ to $l = 150^\circ$ of the Outer arm spiral is a logarithmic spiral, and using the same equation as Reid et al. (2009, 2014) we fitted the spiral of those 457 Outer arm clouds using

$$\ln\left(\frac{R}{R_{\text{ref}}}\right) = -(\beta - \beta_{\text{ref}}) \tan(\psi) \quad (1)$$

where ψ is the spiral pitch angle, β is the galactocentric azimuth (namely the Source-GC-Sun angle), and R_{ref} and β_{ref} are the reference radius and reference azimuth, respectively. The

fitting algorithm is a minimizing chi-square error statistic, and the chi-square error statistic is computed as

$$\chi^2(k, b) = \sum_{i=1}^N W_i (y_i - b - kx_i)^2 \quad (2)$$

where $k = -\tan(\psi)$, $b = \beta_{\text{ref}} \tan(\psi) + \ln(R_{\text{ref}})$, x_i and y_i are β and $\ln(R)$ of each cloud, respectively, and W_i is the weight. The weight is defined as $W = \log_{10}(\frac{M}{M_{\odot}})$.

Fig.2 shows the fitting result. The pitch angle is $\sim 13.1^\circ$, the R_{ref} is ~ 13.6 kpc, the β_{ref} is $\sim 26.9^\circ$ and the χ^2 is ~ 4.1 . Our fitting pitch angle is close to the result of Reid et al. (2014) (pitch= 13.8°), and is consistent with the results of Vallée (2015), who summarized large numbers of recent studies about Milky Way pitch angle and yielded a mean global value of 13.1° .

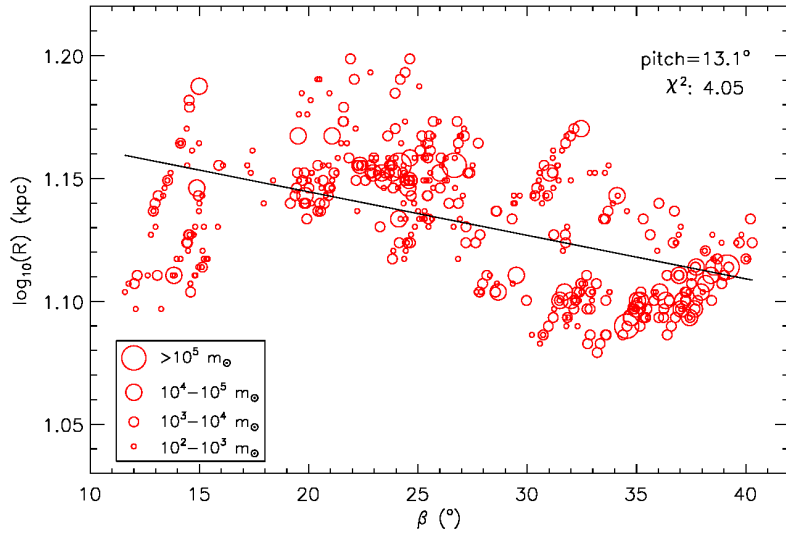


Fig. 2.— Fitting result of the Outer arm pitch angle. R is Galactocentric radius in the units of kpc. β is Galactocentric longitude. Circles indicate molecular clouds of the Outer arm, and their sizes indicate different masses. The fitting line is weighted by mass.

4.2. Plan view

Since Georgelin & Georgelin (1976) presented the famous Milky Way plan view, numerous models have been suggested (see Figure 2 in Steiman-Cameron 2010). Our knowledge about the Milky Way structure has advanced since then a little, so at least the existence of Outer arm is now undoubted, though it was absent in the Georgelin model. In contrast, the lack of arm tracers, especially the remote tracers, still prevent us from knowing more about our galaxy. Thanks to the high-sensitivity CO survey of MWISP, so many molecular clouds of the Outer arm have been detected, and this is the first time that we have detected such large numbers of remote molecular clouds, which contributes a lot to studying the Milky Way structure.

The left panel of Fig. 3 shows the plan view of the Milky Way. The red thick curve indicates the Outer arm spiral fitted by us (hereafter our Outer spiral). Since the Outer arm pitch angle fitted by us is similar to the one fitted by Reid et al. (2014), and their parallax distance of the Outer arm is more precise, we moved our Outer spiral to be parallel to the position of the Reid Outer spiral. Accordingly, the Outer arm clouds are parallelly moved by the same distance. The detailed moving process is as follows: First, using the R_{ref} and β_{ref} fitted by Reid et al. (2014) with the pitch angle fitted by us, we plotted a new spiral curve as the parallel moved curve. Second, we calculated the distance between the new curve and the old curve at every cloud galactic longitude. Third, the new cloud heliocentric distance was calculated as the “old cloud heliocentric distance minus the distance obtained in the second step”. This moving process decreased the cloud heliocentric distances but did not change their longitudes. The right panel of Fig. 3 is the result after the move.

We mentioned these distance biases in 3.2 One may wonder why the kinematic distances obtained from the model that Reid et al. (2014) provided are greater than the distances that they measured. In fact, the biases are mainly caused by errors. Limited parallax data and the parallax measuring errors lead to larger errors of the galactic model. The Reid model narrows the gap between the kinematic distance and the parallax distance but cannot perfectly match them. (And actually, the cloud distances that we moved are roughly below the parallax distance errors. Just see the error bars of the Outer arm HMSFRs in Fig. 3.) Besides, the Reid model is a global model and it is fitted by the maser sources that distribute in almost three galactic quadrants (see Figure 1 of Reid et al. (2014)). But different regions of the Milky Way may have their own peculiar motions. So in different regions the kinematic distances calculated from their model may be a little biased. As a result of these reasons, in the second galactic quadrant (or more exactly in the Outer arm region of the second galactic quadrant) the kinematic distances are a little larger than the parallax distances, just as we see in the left panel of Fig. 3.

Fig. 4 shows the whole view of the Milky Way. We extended our translational (namely the parallel moved) spiral to the inner galaxy. The Reid Outer spiral is also plotted. Additionally, for comparison we plotted two recent fitting results for this arm, of which the arm tracers or fitting methods are different. The cyan dashed curve is one of the fitting results from Hou & Han (2014) (“arm-5” in the third column of Table 4 in their paper). Their arm tracers are HII regions, and their fitting model is the polynomial-logarithmic spiral arm model. The magenta pecked curve is the fitting result from Bobylev & Bajkova (2014). Their arm tracers are 3 HMSFRs and 12 very young star clusters, and their fitting model is the logarithmic spiral. The fact that our translational spiral is located closer to the other three spirals may suggest that the translational locations of the clouds are relatively better. However, this suggestion is not adequate enough to make us revise the distances and other parameters such as mass in Table. 1. The original parameters derived in Sect. 3.2 are retained.

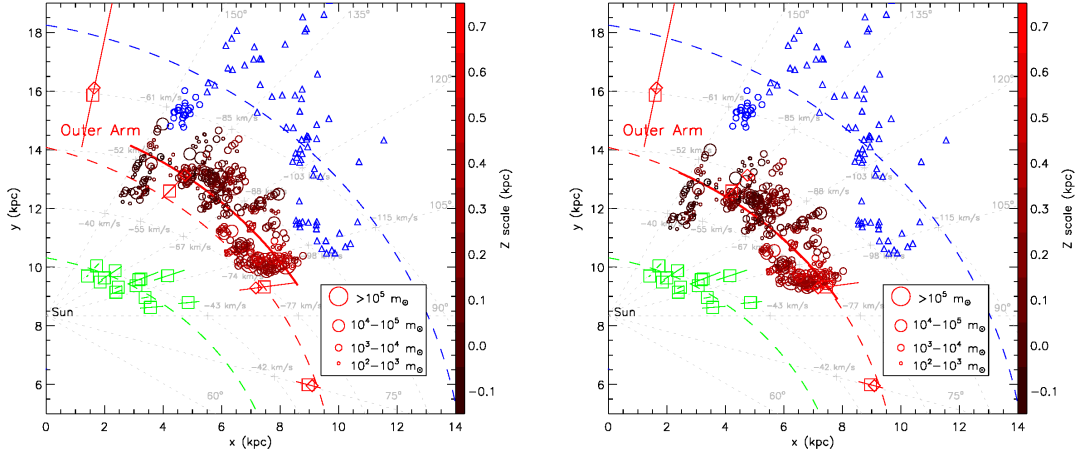


Fig. 3.— (*left panel*) Locations of molecular clouds and HMSFRs in the plan view of the Milky Way. The red and blue circles respectively mark the molecular clouds of the Outer arm and New arm, which are summarized in Table. 1. The blue triangles mark the molecular clouds of the New arm that were detected by Sun et al. (2015). Different sizes of circles and triangles indicate different masses. The red and green squares respectively mark the HMSFRs (Reid et al. 2014) of Outer and Perseus arms. Distance error bars of HMSFRs are indicated. The color depths of the red circles indicate their Z heights. The red diamonds indicate the locations of the Outer arm HMSFRs calculated by kinematic method. The green, red, and blue dashed curves respectively indicate the Reid Perseus spiral, the Reid Outer spiral, and the Sun New spiral. The red thick curve indicates our Outer spiral. The gray dotted curves indicate galactocentric radii=10, 12, 14, 16 kpc. The gray dotted lines indicate galactic longitudes= 60° , 75° , 90° , 105° , 120° , 135° , 150° . The gray crosses and the words beside indicate the locations and the corresponding LSR velocities. (*right panel*) Translational result of the Outer arm clouds and our Outer spiral. For a better comparison, we have not moved or changed any symbols except the red circles and the red thick curve, and the sizes of the red circles remain the same although their masses are changed because of the revised distances.

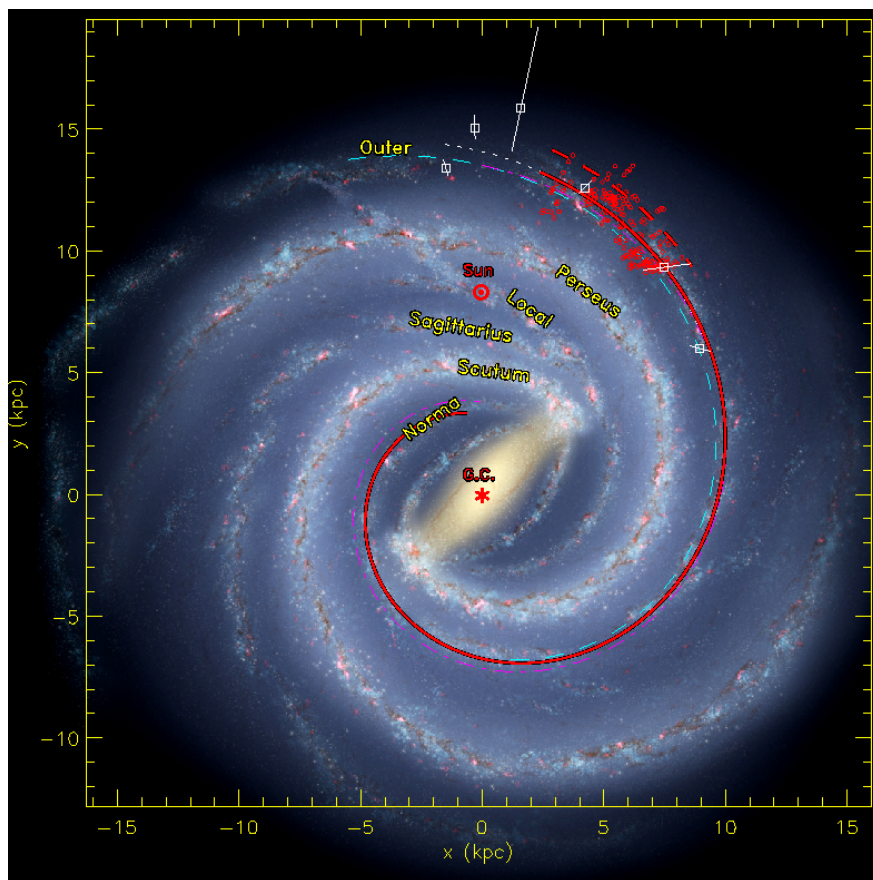


Fig. 4.— An artist’s conception of the Milky Way (R. Hurt: NASA/JPL-Caltech/SSC). The red circles indicate the parallel moved Outer arm clouds with mass $> 10^3 M_{\odot}$. The white squares indicate the Outer arm HMSFRs and the distance error bars are also plotted. The red thick curve indicates the extended translational position of our Outer spiral, and the red thick dashed curve indicates the original position of our Outer spiral. The white dotted curve indicates the Reid Outer spiral. The cyan dashed curve and magenta pecked curve indicate the Outer arm fitting results of Hou & Han (2014) and Bobylev & Bajkova (2014), respectively.

4.3. l - V , V - b and l - b map

Fig. 5 shows the l - V map of HI emission. All the clouds (including the New arm clouds) and HMSFRs are marked on it. Also, the projections of the Reid Outer spiral, the Reid Perseus spiral, the Sun New spiral, and our Outer spiral are plotted. In order to project those spiral curves on the l - V map, or in other words, to convert the dashed curves shown in Fig. 3 into the ones shown in Fig. 5, we compiled a C program on the basis of the FORTRAN code provided by Reid et al. (2009). Their program can calculate the revised heliocentric kinematic distances when inputting the cloud positions and the LSR velocities, just as mentioned in Sect. 3.2. Our program is the inverse — the inputs are cloud position (galactic longitude and latitude) and galactocentric radius, and the output is the LSR velocity. Knowing the expression of the arm curves (namely through Eq. 1), we can obtain an array of galactocentric radii at every galactic longitude. And then, using the Reid model, the coresponding LSR velocities can be calculated by our C program. Using the arrays of longitudes and velocities, we then can plot l - V curves of the arms.

Fig. 6 shows the V - b montage of HI emission. The high-mass Outer arm clouds ($> 10^3 M_\odot$), the New arm clouds, and the HMSFRs are marked on it.

As mentioned in Sect. 3.1, from longitude $l \simeq 100^\circ$ to 120° , there exists an arm-blending region. This phenomenon can be clearly seen from those two figures and may mainly be caused for the following three reasons: (i) Streaming motions near spiral arms have long been predicted by density wave theory and has been observed in other galaxies. (e.g. Figure 4 in Visser 1980, Figure 5 in Aalto et al. 1999) This can probably happen at this region in our galaxy. (ii) Spiral shock may lead to the condition that one LSR velocity could share two different distances. (e.g., Foster & MacWilliams 2006) (iii) The expansion motion of the HI super-bubble near $l = 123^\circ$, $b = -6^\circ$ associated with the Perseus arm may also lead to the velocity mixing. (Sato et al. 2007) Whatever reason mainly causes the mixing LSR velocities, this at least suggests that in this region the gas motion is very peculiar.

Fig. 7 shows the velocity-integrated intensity of HI emission. All the clouds and HMSFRs of the Outer arm are marked on it. Since the velocity ranges of the Outer arm are different at different longitudes, we need to define an $l - V$ function as the integrated velocity window. We have adopted two polynomial fitting curves as the outline of integrated range instead of the spiral $l - V$ projection. This is because the Outer arm velocity ranges are irregular and the polynomial fitting curve is more appropriate for defining the various ranges. The inset of Fig. 7 shows the mass of molecular gas as a function of galactic longitude. The bin is 1 galactic longitude degree. The total mass of all the Outer arm clouds is $\sim 3.1 \times 10^6 M_\odot$. More details about gas distributions are presented in Sect. 4.4.

Those three figures present a 3D view of the arm. The HI and H₂ gases are roughly matched. The warp is obvious.

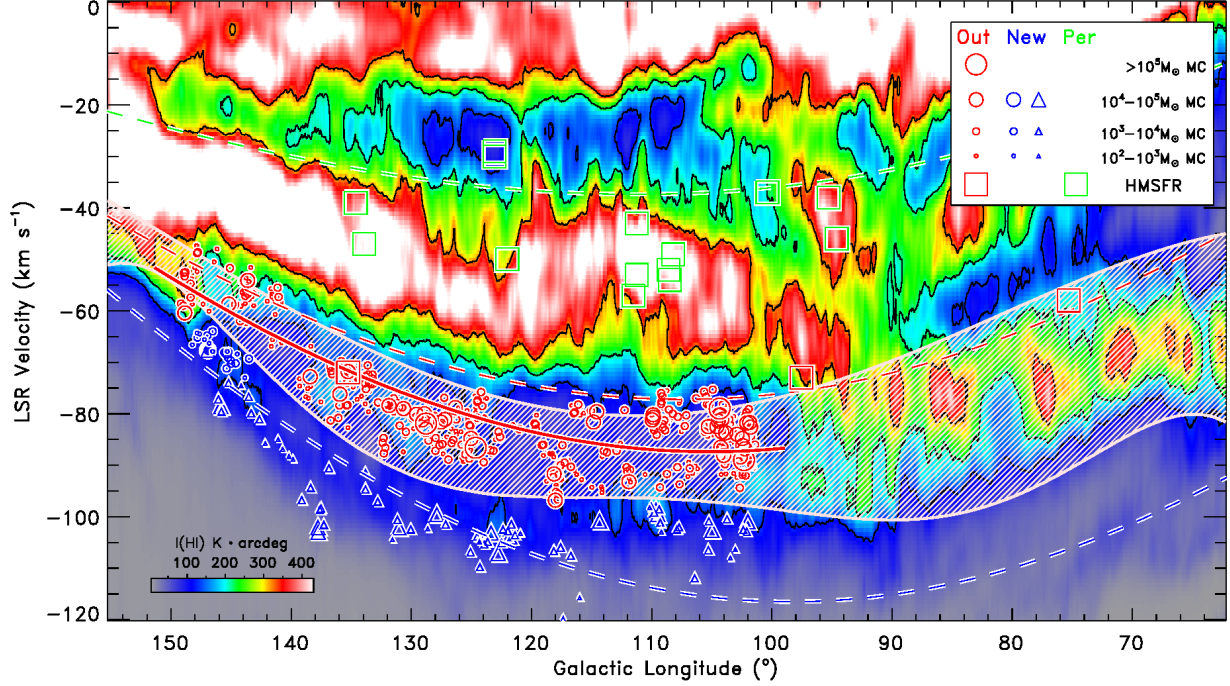


Fig. 5.— Longitude-velocity diagram of HI from the CGPS, integrated over all latitudes (from -3° to 5°). The red and blue circles respectively mark the molecular clouds of the Outer arm and the New arm, which are summarized in Table. 1. The blue triangles mark the molecular clouds of the New arm detected by Sun et al. (2015). Different sizes of circles and triangles indicate different masses. The red and green squares respectively mark the HMSFRs of the Outer and Perseus arms. The green, red, and blue dashed curves respectively indicate the projections of the Reid Perseus spiral, the Reid Outer spiral, and the Sun New spiral. The red thick curve indicates the projection of the Outer arm spiral fitted by us. The pink ribbon indicates the integrated velocity window of Fig. 7.

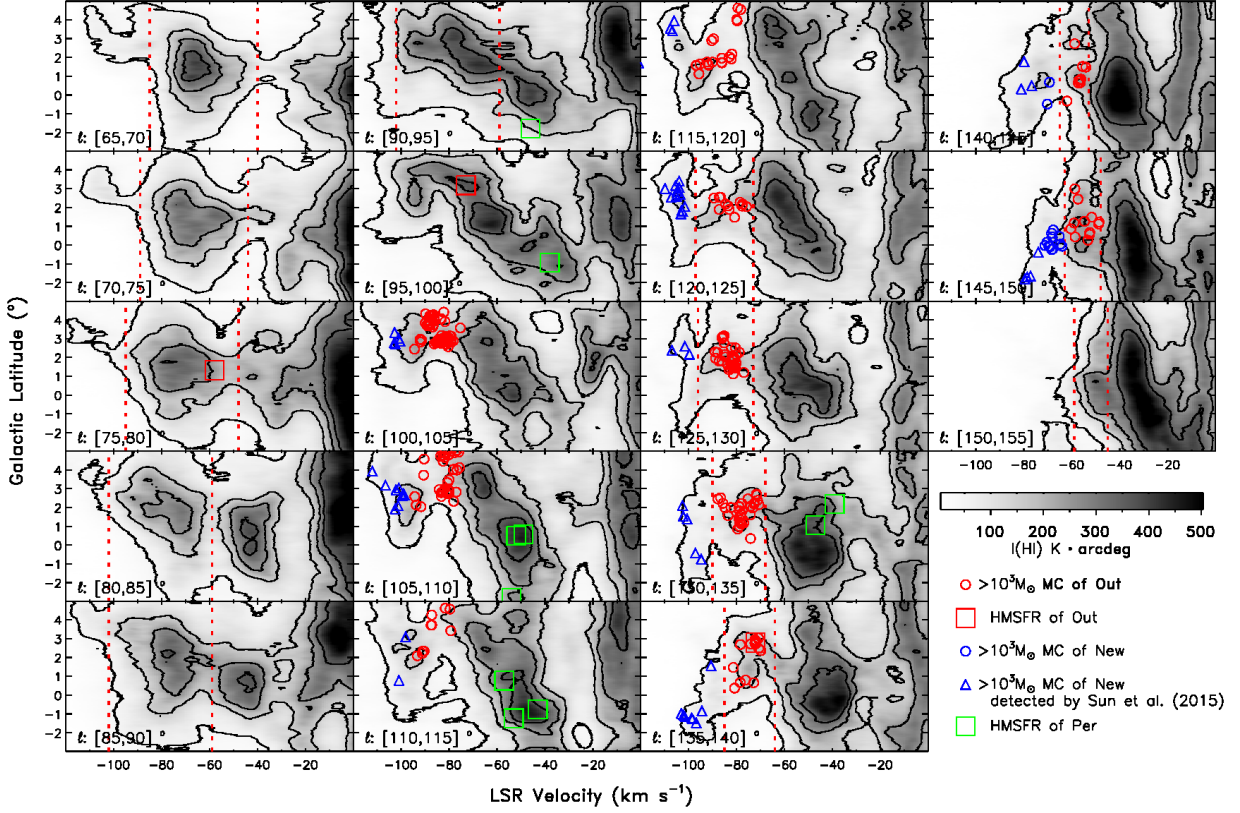


Fig. 6.— Velocity-latitude montage of HI from the CGPS, integrated every 5° of galactic longitude. The Outer arm is embraced in the two dotted red lines in each figure except the figures of the arm-blending region. The meanings of other symbols are consistent with Fig. 5. Note that the low-mass clouds ($< 10^3 M_\odot$) are not plotted, and the symbol size does NOT indicate mass.

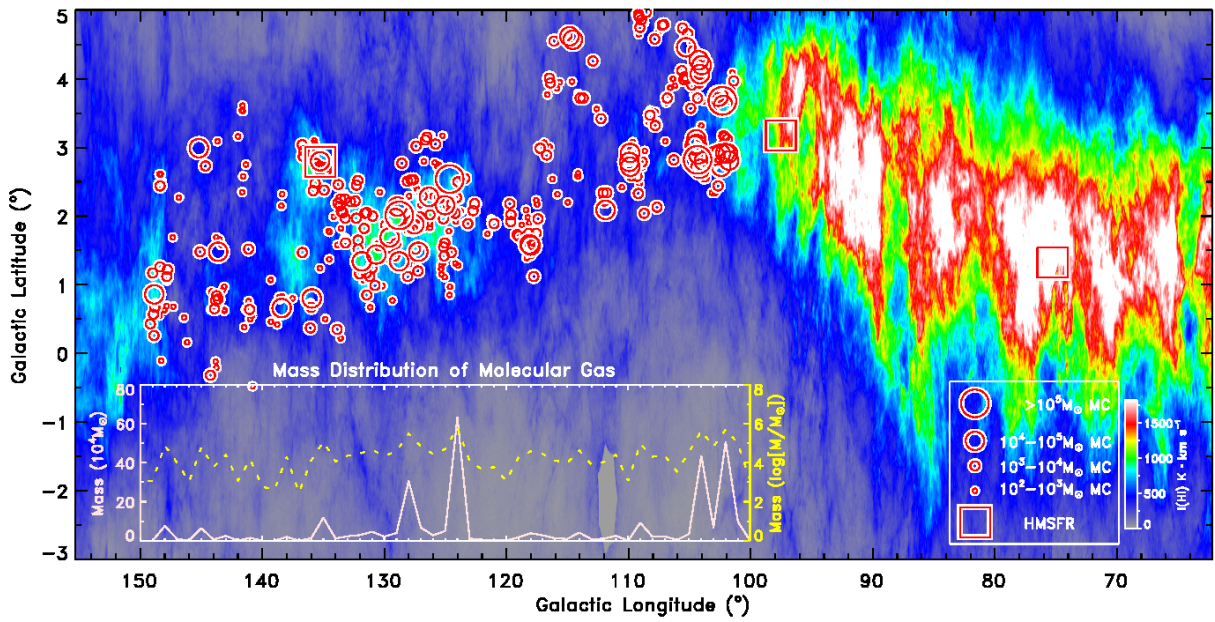


Fig. 7.— Velocity integrated intensity of HI from the CGPS corresponding to the Outer arm. The integrated velocity window is marked by the pink ribbon in Fig. 5. The meanings of the symbols are consistent with Fig. 5. The inset shows the mass of molecular gas as a function of galactic longitude: the solid line and the dashed line correspond to different units.

4.4. Gas distribution

The gas distribution of the Milky Way is a frequently discussed topic. (e.g., Gordon & Burton 1976; Sodroski et al. 1987; Nakanishi & Sofue 2003 and their serial papers; Duarte-Cabral et al. 2015). Whereas, most works often discuss its global distribution (e.g., Burton et al. 1975), only a few have focused on the individual arm (e.g., Grabelsky et al. 1987). Now we present our results of the Outer arm gas distribution.

Fig. 8 shows the Outer arm HI surface density distribution (or column density distribution) along the galactic longitude. Assuming that the 21 cm line is optically thin, the HI surface density is calculated from $\Sigma_{\text{HI}} = 1.82 \times 10^{18} m_{\text{H}} \int T_{\text{B}} dV$, and the column density is calculated by the conversion factor of $1 \text{ M}_{\odot} \text{pc}^{-2} = 1.25 \times 10^{20} \text{ cm}^{-2}$, where m_{H} is the H atom mass, and $\int T_{\text{B}} dV$ is the integrated intensity. The velocity-integrated range is the pink ribbon shown in Fig. 5. Clearly, the HI surface density abruptly descends at $l \simeq 100^{\circ}$, and ascends a little at $l \simeq 120^{\circ}$. The arm-blending region may account for the sharp drop in $l = [100, 120]^{\circ}$, but cannot explain the low surface density region of $l = [120, 155]^{\circ}$. This may suggest that in one spiral arm the gas quantity can largely change. One possible reason may be that: some of the apparent variation in HI surface density could arise from colder, optically thick HI gas, which is known to be widespread in the outer Galaxy, perhaps overlapping with some of the molecular clouds. (see Knee & Brunt 2001, Strasser et al. 2007 and Gibson 2010)

Using the HI surface density and kinematic distance, the HI mass is obtained from the following process. First, since we know the HI surface density at every pixel of the HI integrated map (namely Fig. 7), we then can calculate the mean surface density at every square degree. (This step is somewhat like smoothing the integrated map into a one square degree per pixel map.) Second, using the Reid model we calculate the kinematic distance of every square degree, and the mean LSR velocity of the integrated window (namely the pink ribbon of Fig. 5) at every galactic longitude is used as the LSR velocity of its corresponding square degree. Third, using the kinematic distance and the surface density we can calculate the HI mass in every square degree by $M_{\text{HI}} = \Sigma_{\text{HI}} d_{\text{HI}}^2$, where Σ_{HI} and d_{HI} respectively indicate the surface density and kinematic distance at the corresponding square degree. Fig. 9 shows the HI and H₂ mass distribution along the galactic longitude. (Note that H₂ is different from molecular gas; the latter includes helium.) The bins of HI and H₂ are both 1 galactic longitude degree. The total mass of HI in $l = [63, 155]^{\circ}$, $b = [-3, 5]^{\circ}$ of the Outer arm is $\sim 1.4 \times 10^8 \text{ M}_{\odot}$. And the total mass of H₂ in $l = [100, 150]^{\circ}$, $b = [-3, 5]^{\circ}$ is $\sim 2.3 \times 10^6 \text{ M}_{\odot}$. Since the observation is not fully covered in b , the mass must be higher. The mean mass ratio of H₂ to HI in $l = [100, 150]^{\circ}$, $b = [-3, 5]^{\circ}$ is about 0.1. Fig. 10 shows the HI and H₂ mass distributions along the Z scale in the region of $l = [100, 150]^{\circ}$, $b = [-3, 5]^{\circ}$. About 50%

of the gas mass is included in $Z=[0.2,0.4]$ kpc.

Interestingly, there seems to be a trend in the Z scale distribution (Fig. 10): as the total gas mass becomes large, the H_2 to HI ratio becomes higher. For example, in Fig. 10, at $Z = 0.3$ kpc, the total gas mass is the largest, and accordingly the H_2 to HI ratio is the highest. On the other hand, at $Z = 0.1$ or 0.6 kpc, the gas mass descends and so does the ratio. Also, this trend is visible in the longitude distribution (Fig. 9). One possible explanation may be that although the H_2 distribution is not as diffuse as HI, once it exists, it contributes a lot to the total mass.

It is necessary to emphasize that we are reporting only the mass of H_2 traced by detected CO emission. Significant additional H_2 which CO cannot detect (or say the “CO-dark” H_2 , e.g., Grenier et al. 2005) may also be present. Most of the sight lines plotted in Fig. 8 exceed the minimum column density for self-shielding H_2 (a few times 10^{20} cm^{-2} ; see Snow & McCall 2006 and Sheffer et al. 2008). This is for individual clouds rather than integrated sight lines, but it still seems likely that H_2 could exist in many sightlines where the total HI column is high enough.

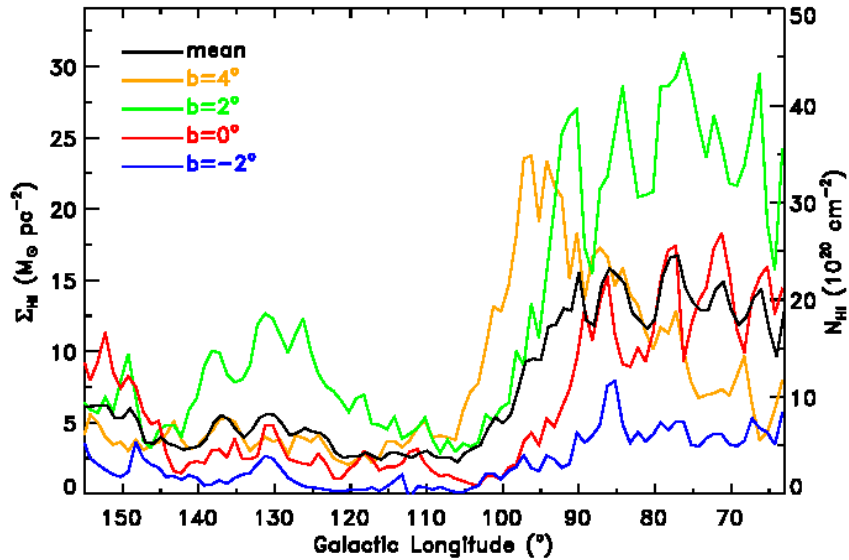


Fig. 8.— Distribution of HI surface density (or column density) of the Outer arm along the galactic longitude. The lines with different colors indicate different galactic latitudes, and the black line indicates the mean value.

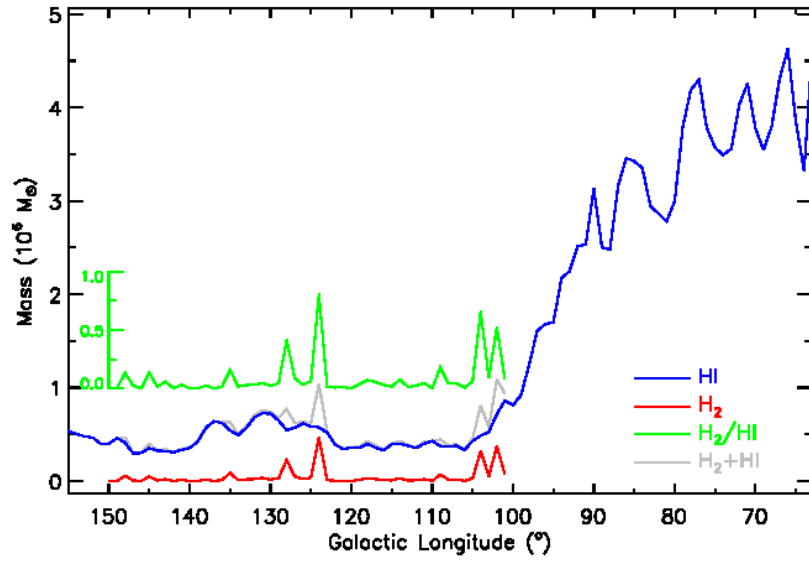


Fig. 9.— Distribution of HI & H_2 masses of the Outer arm along the galactic longitude.

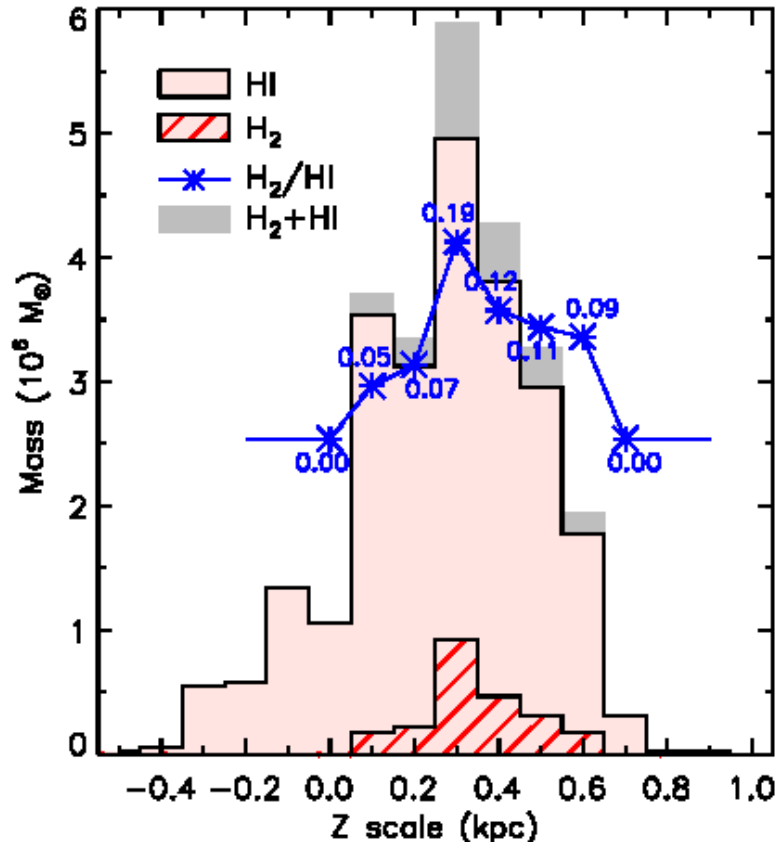


Fig. 10.— Distribution of the HI & H₂ masses along the scale height. This result only shows the region $l = [100, 150]^\circ$, $b = [-3, 5]^\circ$. The blue words beside the asterisks are the mass ratios of H₂ to HI.

4.5. Warp and thickness

Warp is a general phenomenon among disk galaxies. (e.g., Sancisi 1976; Sanchez-Saavedra et al. 1990; Reshetnikov & Combes 1998; García-Ruiz et al. 2002). Additionally, it is one of the most fascinating and important subjects in the study of the Milky Way structure (e.g., Burke 1957; Reed 1996; Momany et al. 2006; López-Corredoira et al. 2010). Figure 3 in the review of Kalberla & Kerp (2009) shows a distinct three-dimensional (3D) picture of the warped Milky Way plane.

In our paper, one can easily notice the Milk Way warp from Fig. 6, 7, 8 and 10. We can roughly obtain a first impression from Fig. 7: the Outer arm starts to bend upward at $l \simeq 80^\circ$, and at $l \simeq 105^\circ$ it reaches its peak and then begins to fall. The whole arm from $l = 63^\circ$ to $l = 155^\circ$ just looks like an arch. In addition, almost all segments of this arch are beyond the $b = 0^\circ$ plane. But since the distance is different at every longitude, the l - b map cannot fully represent the scale height distribution. Now a more detailed analysis is presented. First, we plotted HI mass distributions along the Z scale every 2 galactic longitudes, and H₂ mass distributions every 4 galactic longitudes. Then we fitted every distribution with a Gaussian curve. We define the centric position as the Z scale and the FWHM is the thickness. The final results are shown in Fig. 11. The mean Z scales of the HI layer and the H₂ layer are about 0.31 kpc and 0.25 kpc, respectively. The mean thicknesses of the HI layer and the H₂ layer are about 550 pc and 80 pc, respectively. The Z scales of HI and H₂ are close ($\simeq 0.3$ kpc), but the HI thickness is much larger than that of H₂ (about 7 times thicker, which is not obvious in Fig. 7).

The increasing trend of spiral arm thickness with galactocentric radius has been widely observed and accepted. (e.g., Wouterloot et al. 1990; Kalberla & Kerp 2009). Here we detected a similar trend. Assuming a mean distance of 2 kpc, the HI thickness of the Perseus arm is about 200 pc corresponding to 5° . And as it mentioned above, the Outer arm thickness is about 550 pc. Meanwhile, the thickness of the New arm is 400 to 600 pc (Sun et al. 2015). Obviously the Outer arm is much thicker than the Perseus arm, but is nearly as thick as the New arm. Maybe this provides a little evidence to a trend newly discovered by Honig & Reid (2015) that in the outermost parts of the galaxies some arms become narrow.

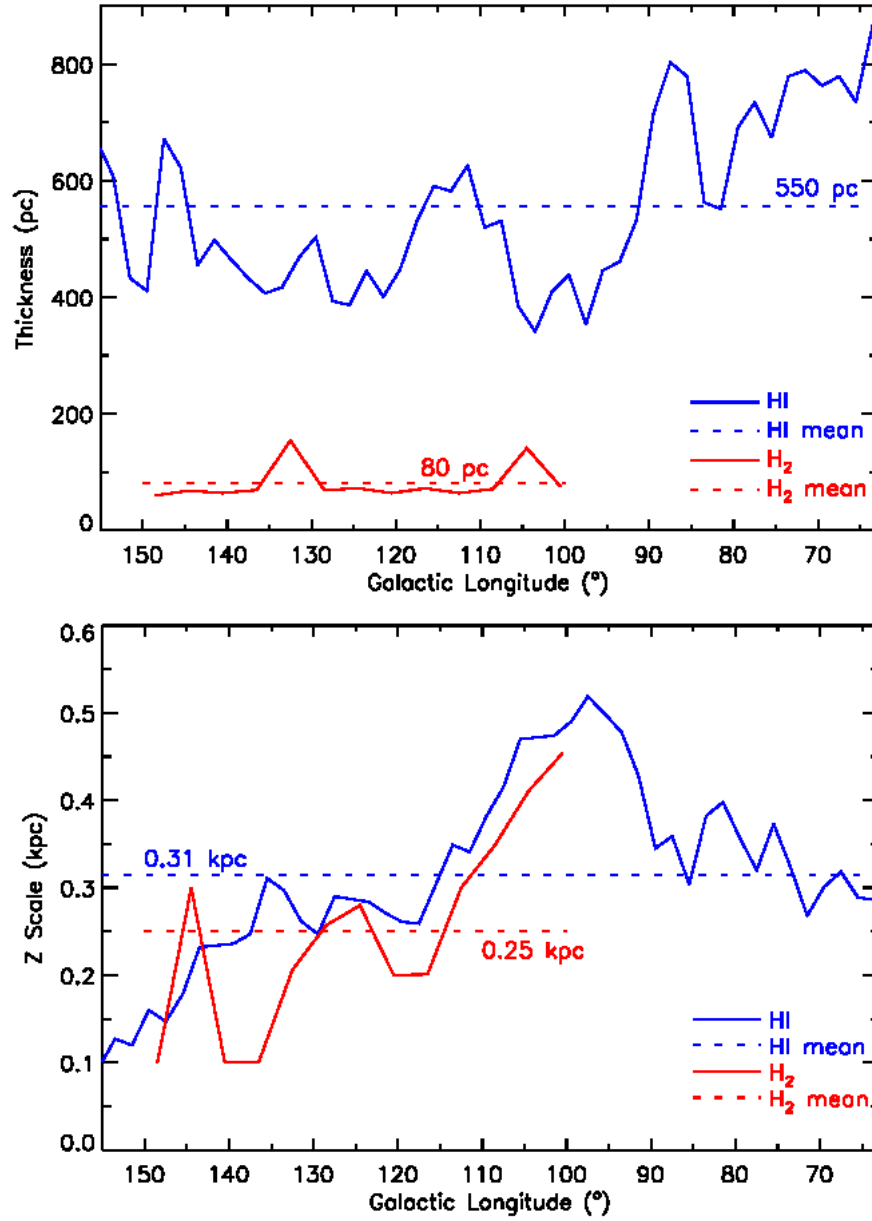


Fig. 11.— Distribution of the Outer arm thickness (*Upper panel*) and scale height (*lower panel*) along the galactic longitude.

5. Summary

Combining 115 GHz $^{12}\text{CO}(1-0)$ data ($l = [100, 150]^\circ$, $b = [-3, 5]^\circ$) of MWISP and 21 cm HI data ($l = [65, 115]^\circ$, $b = [-3, 5]^\circ$) of CGPS, we present the properties of Outer arm in the second galactic quadrant of the Milky Way.

(1) Using CO(1-0), We have detected 481 molecular clouds in total, of which 332 (about 69%) are newly detected, 457 clouds are identified in the Outer arm, and 24 are identified in the New arm. The parameters of all the 481 clouds are summarized in Table. 1.

(2) Assuming that the spiral arm is logarithmic spiral, the pitch angle of the Outer arm is fitted by minimizing chi-square error statistic algorithm, and the result is $\sim 13.1^\circ$.

(3) The total masses of molecular gas and H_2 from $l = 100^\circ$ to 150° in the Outer arm are about $3.1 \times 10^6 M_\odot$ and $2.3 \times 10^6 M_\odot$ respectively. And the total mass of HI gas from $l = 63^\circ$ to 155° is about $1.4 \times 10^8 M_\odot$. Since the observation is not fully covered in b , the mass must be higher. The mean mass ratio of H_2 to HI in $l = [100, 150]^\circ$, $b = [-3, 5]^\circ$ is about 0.1.

(4) The warp of the Outer arm is obvious. The mean Outer arm thicknesses of HI and H_2 are about 550 and 80 pc, respectively, while the scale height of both gases is $\simeq 0.3$ kpc.

We are grateful to all the members of the Milky Way Scroll Painting survey group, especially the staff of the Qinghai Radio Observing Station at Delingha for technical support. Additionally, we gratefully acknowledge the anonymous referee for the helpful and valuable comments. This work is supported by the National Natural Science Foundation of China (grant numbers: 11133008 and 11233007), the Strategic Priority Research Program of the Chinese Academy of Sciences (grant number: XDB09010300), and the Key Laboratory for Radio Astronomy.

REFERENCES

- Aalto, S., Hüttemeister, S., Scoville, N. Z., & Thaddeus, P. 1999, *ApJ*, 522, 165
- Abdo, A. A., Ackermann, M., Ajello, M., et al. 2010, *ApJ*, 710, 133
- Bobylev, V. V., & Bajkova, A. T. 2014, *MNRAS*, 437, 1549
- Bok, B. J., 1959, *The Observatory*, 79, 58
- Brand, J., & Wouterloot, J. G. A. 1994, *A&AS*, 103, 503 s
- Brunt, C. M., Kerton, C. R., & Pomerleau, C. 2003, *ApJS*, 144, 47
- Burke, B. F. 1957, *AJ*, 62, 90
- Burton, W. B., Gordon, M. A., Bania, T. M., & Lockman, F. J. 1975, *ApJ*, 202, 30
- Dame, T. M., Hartmann, D., & Thaddeus, P. 2001, *ApJ*, 547, 792
- Duarte-Cabral, A., Acreman, D. M., Dobbs, C. L., et al. 2015, *MNRAS*, 447, 2144
- Foster, T., & MacWilliams, J. 2006, *ApJ*, 644, 214
- García-Ruiz, I., Sancisi, R., & Kuijken, K. 2002, *A&A*, 394, 769
- Georgelin, Y. M., & Georgelin, Y. P. 1976, *A&A*, 49, 57
- Gibson, S. J. 2010, *The Dynamic Interstellar Medium: A Celebration of the Canadian Galactic Plane Survey*, 438, 111
- Gordon, M. A., & Burton, W. B. 1976, *ApJ*, 208, 346
- Grabelsky, D. A., Cohen, R. S., Bronfman, L., Thaddeus, P., & May, J. 1987, *ApJ*, 315, 122
- Grenier, I. A., Casandjian, J.-M., & Terrier, R. 2005, *Science*, 307, 1292
- Hachisuka, K., Choi, Y. K., Reid, M. J., et al. 2015, *ApJ*, 800, 2
- Henderson, A. P., Jackson, P. D., & Kerr, F. J. 1982, *ApJ*, 263, 116
- Heyer, M. H., Brunt, C., Snell, R. L., et al. 1998, *ApJS*, 115, 241
- Heyer, M. H., Carpenter, J. M., & Snell, R. L. 2001, *ApJ*, 551, 852
- Hildebrand, R. H. 1983, *QJRAS*, 24, 267

- Honig, Z. N., & Reid, M. J. 2015, *ApJ*, 800, 53
- Hou, L. G., & Han, J. L. 2014, *A&A*, 569, A125
- Kalberla, P. M. W., & Kerp, J. 2009, *ARA&A*, 47, 27
- Knee, L. B. G., & Brunt, C. M. 2001, *Nature*, 412, 308
- Ladd, E. F., Myers, P. C., & Goodman, A. A. 1994, *ApJ*, 433, 117
- López-Corredoira, M., Cabrera-Lavers, A., Hammersley, P. L., et al. 2010, *Highlights of Astronomy*, 15, 811
- Moffat, A. F. J., & Vogt, N. 1975, *A&AS*, 20, 85
- Momany, Y., Zaggia, S., Gilmore, G., et al. 2006, *A&A*, 451, 515
- Nakanishi, H., & Sofue, Y. 2003, *PASJ*, 55, 191
- Negueruela, I., & Marco, A. 2003, *A&A*, 406, 119
- Oort, J. H., Kerr, F. J., Westerhout, G. 1958, *MNRAS*, 118, 379
- Reed, B. C. 1996, *AJ*, 111, 804
- Reid, M. J., Menten, K. M., Zheng, X. W., et al. 2009, *ApJ*, 700, 137
- Reid, M. J., Menten, K. M., Brunthaler, A., et al. 2014, *ApJ*, 783, 130
- Reshetnikov, V., & Combes, F. 1998, *A&A*, 337, 9
- Russeil, D. 2003, *A&A*, 397, 133
- Russeil, D., Adami, C., & Georgelin, Y. M. 2007, *A&A*, 470, 161
- Sanchez-Saavedra, M. L., Battaner, E., & Florido, E. 1990, *MNRAS*, 246, 458
- Sancisi, R. 1976, *A&A*, 53, 159
- Sato, M., Hirota, T., Honma, M., et al. 2007, *PASJ*, 59, 743
- Shan, W.L., Yang, J., Shi, S. C., et al. 2012, *IEEE Transactions on Terahertz Science and Technology*, 2,593
- Sheffer, Y., Rogers, M., Federman, S. R., et al. 2008, *ApJ*, 687, 1075
- Snow, T. P., & McCall, B. J. 2006, *ARA&A*, 44, 367

- Sodroski, T. J., Dwek, E., Hauser, M. G., & Kerr, F. J. 1987, *ApJ*, 322, 101
- Steiman-Cameron, T. Y. 2010, *Galaxies and their Masks*, 45
- Strasser, S. T., Dickey, J. M., Taylor, A. R., et al. 2007, *AJ*, 134, 2252
- Sun, Y., Xu, Y., Yang, J., et al. 2015, *ApJ*, 798, L27
- Taylor, J. H., & Cordes, J. M. 1993, *ApJ*, 411, 674
- Taylor, A. R., Gibson, S. J., Peracaula, M., et al. 2003, *AJ*, 125, 3145
- Vallée, J. P. 2008, *AJ*, 135, 1301
- Vallée, J. P. 2015, *MNRAS*, 450, 4277
- Visser, H. C. D. 1980, *A&A*, 88, 159
- Wouterloot, J. G. A., Brand, J., Burton, W. B., & Kwee, K. K. 1990, *A&A*, 230, 21
- Xu, Y., Reid, M. J., Zheng, X. W., & Menten, K. M. 2006, *Science*, 311, 54

Table 1. Parameters of molecular clouds derived by CO(1-0)

Name	V_{LSR} (km s^{-1})	T_{peak} (K)	ΔV (km s^{-1})	I_{CO} ($\text{K} \cdot \text{km s}^{-1}$)	Area (arcmin^2)	d (kpc)	R (kpc)	Size (pc)	Mass ($10^3 M_{\odot}$)	Z Scale (kpc)	Note
(1)	(2)	(3)	(4)	(5)	(6)	(7)	(8)	(9)	(10)	(11)	(12)
MWISP G101.400+03.967	-86.0	2.3	1.6	3.9	15.4	8.2	12.8	10.4	1.3	0.6	
MWISP G101.508+04.092	-90.5	3.2	1.1	3.6	3.0	8.6	13.1	4.4	0.2	0.6	
MWISP G101.633+02.867	-82.6	3.6	1.6	6.2	10.0	7.8	12.5	7.9	1.2	0.4	
MWISP G101.683+02.917	-81.7	4.4	1.3	5.9	21.7	7.7	12.4	11.6	2.5	0.4	
MWISP G101.700+03.833	-89.9	7.9	1.4	11.5	25.8	8.6	13.1	14.2	7.4	0.6	
MWISP G101.708+02.867	-84.3	4.9	1.2	6.3	18.4	8.0	12.6	11.1	2.5	0.4	
MWISP G101.767+02.808	-82.6	16.5	2.9	51.0	43.3	7.8	12.5	16.7	45.8	0.4	
MWISP G101.800+02.958	-81.4	2.5	0.7	2.0	4.8	7.7	12.4	5.2	0.2	0.4	
MWISP G101.808+03.817	-88.0	2.2	1.6	3.9	18.5	8.3	12.9	11.5	1.7	0.6	
MWISP G101.850+02.908	-81.7	7.7	2.0	16.1	40.4	7.7	12.4	15.9	13.1	0.4	
MWISP G101.900+03.708	-89.0	2.4	1.9	5.3	38.4	8.4	13.0	17.0	4.9	0.5	
MWISP G101.917+03.117	-79.1	5.2	2.0	10.8	47.0	7.4	12.2	16.5	9.5	0.4	
MWISP G101.983+02.900	-83.1	6.6	1.7	11.6	35.1	7.8	12.6	15.0	8.4	0.4	
MWISP G102.008+02.833	-82.1	3.3	1.2	4.5	6.6	7.7	12.5	6.2	0.6	0.4	
MWISP G102.033+02.800	-85.3	3.2	0.9	3.0	6.4	8.0	12.7	6.3	0.4	0.4	
MWISP G102.083+02.917	-81.8	6.0	1.6	10.3	55.6	7.7	12.5	18.7	11.6	0.4	
MWISP G102.117+03.150	-79.7	3.5	1.3	4.8	12.3	7.5	12.3	8.4	1.1	0.4	
MWISP G102.150+03.708	-87.8	2.6	1.3	3.7	22.8	8.3	12.9	12.8	2.0	0.5	
MWISP G102.183+02.967	-84.1	4.5	1.4	7.0	18.5	7.9	12.6	11.0	2.7	0.4	
MWISP G102.192+02.967	-92.0	4.5	1.2	5.7	18.4	8.8	13.3	12.2	2.7	0.5	
MWISP G102.208+03.167	-83.1	3.6	1.0	3.7	15.3	7.8	12.6	9.8	1.1	0.4	
MWISP G102.217+03.050	-80.5	4.3	1.4	6.3	30.2	7.5	12.4	13.4	3.6	0.4	
MWISP G102.250+03.617	-86.8	4.8	1.6	8.1	60.0	8.2	12.9	20.7	11.2	0.5	
MWISP G102.258+02.917	-82.0	4.2	1.4	6.1	20.8	7.7	12.5	11.4	2.5	0.4	
MWISP G102.317+03.683	-89.0	11.6	3.3	41.0	263.5	8.4	13.0	44.7	262.6	0.5	
MWISP G102.342+02.883	-81.1	3.3	2.0	7.0	38.5	7.6	12.4	15.4	5.3	0.4	
MWISP G102.417+02.717	-86.2	5.4	2.0	11.9	174.0	8.1	12.8	35.0	46.7	0.4	
MWISP G102.433+02.917	-91.4	3.5	1.0	3.7	21.5	8.7	13.3	13.1	2.0	0.4	
MWISP G102.442+02.833	-91.9	5.1	0.7	3.6	10.9	8.7	13.3	9.2	1.0	0.4	
MWISP G102.450+02.908	-84.8	4.4	2.4	11.3	118.9	8.0	12.7	28.6	29.5	0.4	
MWISP G102.600+02.917	-84.1	2.5	1.2	3.3	13.7	7.9	12.7	9.4	0.9	0.4	
MWISP G102.633+03.742	-88.4	5.6	1.9	11.5	187.6	8.3	13.0	37.3	51.2	0.5	BKP03
MWISP G102.667+02.442	-94.4	2.6	1.4	3.8	15.2	9.0	13.6	11.3	1.6	0.4	
MWISP G102.742+03.733	-89.2	4.0	1.5	6.5	52.5	8.4	13.1	19.9	8.2	0.5	
MWISP G102.817+03.717	-89.2	4.6	1.6	7.9	18.6	8.4	13.1	11.7	3.5	0.5	BKP03
MWISP G102.900+02.883	-84.0	5.0	2.1	11.2	213.8	7.8	12.6	37.4	50.2	0.4	BKP03
MWISP G102.908+02.342	-92.4	3.2	1.2	4.2	6.1	8.8	13.4	6.8	0.6	0.4	
MWISP G102.992+02.792	-85.5	3.2	2.1	7.3	33.9	8.0	12.8	15.2	5.4	0.4	
MWISP G103.067+02.800	-85.1	4.1	1.4	6.1	14.2	7.9	12.7	9.6	1.8	0.4	BKP03
MWISP G103.167+02.342	-91.6	2.2	1.0	2.2	2.7	8.7	13.3	4.1	0.1	0.4	
MWISP G103.167+02.942	-80.5	1.9	1.5	3.0	6.0	7.4	12.4	5.6	0.3	0.4	
MWISP G103.267+02.742	-83.1	3.7	2.8	10.6	10.7	7.7	12.6	8.0	2.2	0.4	BKP03
MWISP G103.408+02.867	-84.7	2.5	1.9	5.1	29.8	7.9	12.7	14.0	3.2	0.4	BKP03
MWISP G103.467+02.808	-82.1	4.9	1.7	8.9	48.9	7.6	12.5	17.3	8.6	0.4	BKP03

Table 1—Continued

Name	V_{LSR} (km s^{-1})	T_{peak} (K)	ΔV (km s^{-1})	I_{CO} ($\text{K} \cdot \text{km s}^{-1}$)	Area (arcmin^2)	d (kpc)	R (kpc)	Size (pc)	Mass ($10^3 M_{\odot}$)	Z Scale (kpc)	Note
(1)	(2)	(3)	(4)	(5)	(6)	(7)	(8)	(9)	(10)	(11)	(12)
MWISP G103.467+02.858	-84.8	3.9	1.0	4.3	17.0	7.9	12.7	10.5	1.5	0.4	
MWISP G103.542+02.842	-81.1	3.5	2.2	7.8	22.4	7.5	12.4	11.5	3.3	0.4	BKP03
MWISP G103.792+02.567	-80.4	4.2	2.0	8.9	25.6	7.4	12.4	12.1	4.2	0.3	
MWISP G103.817+04.150	-91.7	2.5	1.1	2.8	6.0	8.6	13.3	6.6	0.4	0.6	
MWISP G103.833+03.667	-89.6	3.1	1.2	4.1	8.6	8.4	13.1	7.8	0.8	0.5	
MWISP G103.842+02.800	-83.7	4.6	4.2	20.5	75.3	7.7	12.7	21.8	31.4	0.4	
MWISP G103.900+02.800	-80.6	4.1	1.5	7.0	31.1	7.4	12.4	13.4	4.0	0.4	
MWISP G103.908+04.317	-89.8	2.9	1.8	5.4	40.6	8.4	13.2	17.4	5.3	0.6	
MWISP G104.000+02.867	-79.5	2.4	1.6	4.2	14.2	7.3	12.3	8.8	1.1	0.4	BKP03
MWISP G104.008+04.200	-88.1	8.7	3.4	30.7	64.9	8.2	13.0	21.6	45.8	0.6	BKP03
MWISP G104.050+03.317	-89.9	2.4	1.3	3.4	4.3	8.4	13.2	5.3	0.3	0.5	
MWISP G104.067+02.892	-78.2	3.4	2.0	7.6	32.7	7.1	12.2	13.2	4.2	0.4	
MWISP G104.083+04.250	-87.2	3.9	1.8	7.4	52.0	8.1	12.9	19.1	8.6	0.6	
MWISP G104.092+04.042	-83.2	2.9	2.8	8.5	35.5	7.6	12.6	14.7	5.9	0.5	
MWISP G104.150+02.692	-81.1	7.8	2.8	23.5	109.3	7.4	12.5	25.3	48.3	0.3	BKP03
MWISP G104.167+04.067	-83.5	3.7	1.6	6.2	88.3	7.7	12.6	23.7	11.1	0.5	BKP03
MWISP G104.208+03.942	-88.3	3.1	1.2	3.8	24.0	8.2	13.0	13.0	2.1	0.6	
MWISP G104.217+03.117	-91.8	2.6	1.0	2.7	3.9	8.6	13.4	5.1	0.2	0.5	
MWISP G104.217+04.092	-86.2	3.1	1.9	6.1	8.8	8.0	12.9	7.5	1.1	0.6	BKP03
MWISP G104.250+02.917	-79.3	5.2	1.8	10.2	34.0	7.2	12.3	13.7	6.1	0.4	
MWISP G104.250+04.267	-86.5	3.8	2.4	9.8	324.8	8.0	12.9	47.3	70.2	0.6	
MWISP G104.292+02.900	-80.2	8.2	2.6	22.2	29.3	7.3	12.4	12.8	11.7	0.4	BKP03
MWISP G104.333+04.058	-86.1	2.2	2.0	4.6	30.3	7.9	12.9	14.1	2.9	0.6	
MWISP G104.350+02.817	-79.0	11.5	2.4	29.3	267.0	7.2	12.3	38.6	139.7	0.4	
MWISP G104.350+03.717	-86.6	3.5	1.5	5.7	33.0	8.0	12.9	14.9	4.1	0.5	
MWISP G104.417+03.050	-80.3	6.0	2.9	18.3	73.3	7.3	12.4	20.4	24.5	0.4	BKP03
MWISP G104.458+03.117	-81.4	8.4	2.5	21.8	53.5	7.4	12.5	17.7	21.8	0.4	BKP03
MWISP G104.467+02.950	-80.6	5.4	1.8	10.5	11.2	7.4	12.4	7.9	2.1	0.4	
MWISP G104.583+03.033	-82.5	4.3	3.5	15.5	41.5	7.5	12.6	15.7	12.3	0.4	
MWISP G104.617+03.767	-81.5	2.5	0.9	2.5	3.4	7.4	12.5	4.1	0.1	0.5	
MWISP G104.700+04.408	-82.2	1.8	2.2	4.2	63.7	7.5	12.5	19.6	5.1	0.6	
MWISP G104.758+04.100	-82.5	1.9	1.0	2.1	8.7	7.5	12.6	7.0	0.3	0.5	
MWISP G104.817+03.908	-81.7	1.8	1.4	2.7	60.8	7.4	12.5	18.8	3.1	0.5	
MWISP G104.817+04.517	-84.1	1.7	1.9	3.5	10.8	7.7	12.7	8.1	0.7	0.6	
MWISP G104.917+03.567	-75.3	2.9	1.6	5.2	16.8	6.8	12.0	9.0	1.3	0.4	BKP03
MWISP G104.958+03.908	-81.1	2.2	0.8	2.0	25.7	7.4	12.5	12.2	0.9	0.5	
MWISP G105.167+04.658	-81.8	2.6	1.9	5.3	68.5	7.4	12.5	20.0	6.8	0.6	
MWISP G105.217+04.000	-78.2	2.4	1.7	4.3	21.2	7.0	12.2	10.4	1.5	0.5	
MWISP G105.292+04.458	-82.5	2.5	2.7	7.6	86.3	7.5	12.6	22.8	12.7	0.6	
MWISP G105.342+04.608	-84.4	1.4	1.7	2.6	14.1	7.7	12.7	9.3	0.7	0.6	
MWISP G105.400+04.033	-78.1	2.4	2.2	5.6	56.3	7.0	12.2	17.1	5.3	0.5	
MWISP G105.450+04.608	-83.0	1.1	1.5	2.0	11.4	7.5	12.6	8.1	0.4	0.6	
MWISP G105.483+03.992	-76.7	3.3	1.8	6.4	45.7	6.9	12.1	15.2	4.7	0.5	BKP03
MWISP G105.583+04.742	-83.5	1.7	1.8	3.5	18.9	7.6	12.7	10.7	1.3	0.6	

Table 1—Continued

Name	V_{LSR} (km s^{-1})	T_{peak} (K)	ΔV (km s^{-1})	I_{CO} ($\text{K} \cdot \text{km s}^{-1}$)	Area (arcmin^2)	d (kpc)	R (kpc)	Size (pc)	Mass ($10^3 M_{\odot}$)	Z Scale (kpc)	Note
(1)	(2)	(3)	(4)	(5)	(6)	(7)	(8)	(9)	(10)	(11)	(12)
MWISP G105.642+04.117	-75.7	2.7	1.5	4.5	35.5	6.8	12.1	13.2	2.5	0.5	
MWISP G106.192+03.900	-90.7	2.9	1.0	3.1	7.5	8.3	13.3	7.2	0.5	0.6	
MWISP G106.300+02.817	-77.0	2.5	2.5	6.3	11.8	6.9	12.2	7.6	1.2	0.3	
MWISP G106.367+04.000	-90.2	2.4	1.0	2.5	2.8	8.3	13.3	4.1	0.1	0.6	
MWISP G106.592+03.867	-91.6	1.7	0.7	1.3	4.6	8.4	13.4	5.5	0.1	0.6	
MWISP G106.833+03.717	-90.6	3.7	0.6	2.3	25.8	8.3	13.3	13.7	1.4	0.5	HCS01;BKP03
MWISP G106.917+03.650	-89.4	3.1	0.4	1.4	3.4	8.1	13.2	4.5	0.1	0.5	
MWISP G106.992+03.092	-92.2	2.8	0.6	1.7	3.1	8.5	13.5	4.4	0.1	0.5	
MWISP G107.133+04.792	-80.3	1.6	3.3	5.6	50.6	7.1	12.5	16.5	4.9	0.6	
MWISP G107.250+04.783	-82.4	1.9	1.7	3.5	42.8	7.3	12.6	15.6	2.7	0.6	HCS01
MWISP G107.408+04.717	-82.7	1.8	1.6	3.0	7.1	7.4	12.7	6.2	0.4	0.6	
MWISP G107.517+04.692	-83.5	2.7	1.1	3.1	10.3	7.4	12.7	7.6	0.6	0.6	
MWISP G107.667+03.317	-77.4	2.1	1.1	2.6	5.1	6.8	12.3	4.7	0.2	0.4	
MWISP G107.683+02.133	-93.7	4.0	1.3	5.5	13.1	8.6	13.7	10.0	1.8	0.3	BKP03
MWISP G107.708+03.367	-77.9	2.8	1.1	3.3	11.5	6.9	12.3	7.5	0.6	0.4	BKP03
MWISP G107.800+03.517	-81.3	2.5	1.1	2.9	6.8	7.2	12.6	5.9	0.3	0.4	
MWISP G107.817+03.317	-80.6	2.0	4.9	10.3	40.8	7.1	12.5	14.8	7.2	0.4	
MWISP G107.858+04.583	-90.4	3.5	1.3	4.6	43.4	8.2	13.4	17.6	4.6	0.7	HCS01;BKP03
MWISP G108.217+03.542	-80.8	2.3	2.0	4.8	9.1	7.1	12.6	6.8	0.7	0.4	
MWISP G108.242+03.467	-80.0	3.0	0.9	3.2	33.8	7.0	12.5	13.2	1.8	0.4	
MWISP G108.367+03.367	-79.1	1.5	0.8	1.5	37.3	6.9	12.4	13.7	0.9	0.4	
MWISP G108.558+04.967	-79.2	3.6	1.2	4.6	37.0	6.9	12.4	13.7	2.8	0.6	BKP03
MWISP G108.683+02.950	-82.0	2.6	1.2	3.5	7.7	7.2	12.7	6.3	0.4	0.4	
MWISP G108.717+04.817	-75.5	3.5	0.7	2.6	16.5	6.5	12.1	8.5	0.6	0.5	
MWISP G108.733+02.042	-91.7	5.4	1.4	8.0	9.9	8.3	13.6	8.3	1.8	0.3	BKP03
MWISP G108.800+02.833	-82.1	3.8	0.6	2.4	4.6	7.3	12.7	4.8	0.2	0.4	
MWISP G108.867+02.708	-83.0	1.9	1.0	2.1	8.7	7.3	12.8	6.8	0.3	0.3	
MWISP G108.883+02.792	-83.2	4.5	2.1	10.2	46.7	7.4	12.8	16.5	8.9	0.4	HCS01;BKP03
MWISP G108.950+04.858	-81.3	5.3	1.1	6.0	21.1	7.1	12.6	10.6	2.1	0.6	HCS01;BKP03
MWISP G109.067+05.058	-78.9	2.9	0.9	2.7	6.8	6.9	12.4	5.6	0.3	0.6	
MWISP G109.083+04.750	-82.7	2.6	1.2	3.2	20.0	7.3	12.7	10.6	1.1	0.6	
MWISP G109.100+04.900	-82.0	2.6	0.9	2.5	22.8	7.2	12.7	11.1	1.0	0.6	
MWISP G109.108+02.467	-80.8	2.7	1.4	4.0	7.0	7.1	12.6	5.9	0.4	0.3	
MWISP G109.117+05.058	-76.6	3.6	1.9	7.2	21.7	6.6	12.2	10.0	2.3	0.6	BKP03
MWISP G109.158+04.650	-81.5	2.1	1.5	3.4	7.9	7.1	12.6	6.3	0.4	0.6	
MWISP G109.167+04.917	-77.6	4.8	2.6	13.3	16.4	6.7	12.3	8.7	3.3	0.6	HCS01;BKP03
MWISP G109.167+04.967	-76.0	4.4	2.3	10.9	4.0	6.6	12.2	4.0	0.6	0.6	
MWISP G109.183+04.892	-75.6	3.0	0.7	2.3	6.4	6.5	12.2	5.1	0.2	0.6	
MWISP G109.200+04.942	-76.0	5.6	1.5	8.8	7.8	6.6	12.2	5.8	1.0	0.6	
MWISP G109.208+02.333	-78.1	4.4	1.1	5.4	41.4	6.8	12.4	14.3	3.5	0.3	BKP03
MWISP G109.308+02.583	-94.3	3.3	1.2	4.4	19.5	8.6	13.8	12.3	2.1	0.4	BKP03
MWISP G109.583+02.950	-84.1	2.9	2.1	6.5	24.1	7.4	12.9	11.8	2.9	0.4	
MWISP G109.658+03.083	-82.7	2.3	1.3	3.2	13.0	7.3	12.8	8.4	0.7	0.4	BKP03
MWISP G109.683+02.983	-81.9	2.1	2.7	5.9	21.5	7.2	12.7	10.8	2.2	0.4	

Table 1—Continued

Name	V_{LSR} (km s^{-1})	T_{peak} (K)	ΔV (km s^{-1})	I_{CO} ($\text{K} \cdot \text{km s}^{-1}$)	Area (arcmin^2)	d (kpc)	R (kpc)	Size (pc)	Mass ($10^3 M_{\odot}$)	Z Scale (kpc)	Note
(1)	(2)	(3)	(4)	(5)	(6)	(7)	(8)	(9)	(10)	(11)	(12)
MWISP G109.792+02.592	-83.2	3.2	2.1	7.1	15.6	7.3	12.8	9.3	2.0	0.3	
MWISP G109.817+02.833	-82.6	4.9	1.8	9.5	47.7	7.3	12.8	16.4	8.2	0.4	
MWISP G109.858+02.717	-80.7	10.9	2.5	28.9	45.5	7.1	12.6	15.6	22.6	0.3	HCS01
MWISP G109.883+02.917	-80.2	5.0	3.6	19.3	36.9	7.0	12.6	13.8	11.9	0.4	HCS01;BKP03
MWISP G109.950+02.792	-81.2	6.5	1.9	13.0	77.0	7.1	12.7	20.4	17.3	0.3	BKP03
MWISP G109.983+02.992	-80.0	2.0	1.2	2.7	19.5	7.0	12.6	10.0	0.9	0.4	
MWISP G109.992+02.833	-79.9	5.0	2.2	11.8	38.9	7.0	12.6	14.2	7.6	0.3	HCS01
MWISP G110.067+02.792	-79.5	2.4	1.5	3.7	7.8	6.9	12.5	6.1	0.4	0.3	
MWISP G110.550+02.417	-91.8	3.5	1.2	4.5	7.9	8.3	13.7	7.4	0.8	0.4	HCS01;BKP03
MWISP G111.758+02.250	-93.3	2.9	1.4	4.4	4.7	8.4	13.9	5.6	0.4	0.3	
MWISP G111.800+02.342	-90.9	3.1	0.8	2.7	23.3	8.1	13.6	12.7	1.4	0.3	HCS01;BKP03
MWISP G111.892+02.092	-93.2	5.3	2.1	11.9	79.0	8.4	13.9	24.4	22.7	0.3	HCS01;BKP03
MWISP G111.892+02.183	-92.5	3.5	1.1	4.0	10.3	8.3	13.8	8.5	0.9	0.3	
MWISP G112.033+02.217	-91.2	3.4	0.8	3.0	27.8	8.2	13.7	14.0	1.9	0.3	HCS01
MWISP G112.092+02.342	-90.4	2.9	0.9	2.6	26.8	8.1	13.6	13.6	1.5	0.3	BKP03
MWISP G112.258+03.417	-79.3	2.8	2.2	6.2	19.9	6.8	12.6	9.8	1.9	0.4	
MWISP G112.608+03.558	-85.7	2.1	0.9	1.9	8.7	7.5	13.2	7.0	0.3	0.5	
MWISP G112.917+04.258	-87.2	3.6	1.3	5.4	50.3	7.6	13.3	17.6	5.4	0.6	HCS01;BKP03
MWISP G113.717+03.717	-87.5	2.7	1.9	5.6	21.7	7.7	13.4	11.6	2.4	0.5	HCS01;BKP03
MWISP G113.967+03.717	-87.2	3.8	1.6	6.4	44.0	7.6	13.4	16.4	5.5	0.5	HCS01
MWISP G114.117+02.583	-94.6	3.4	1.0	3.5	9.0	8.6	14.2	8.2	0.8	0.4	
MWISP G114.117+03.783	-88.3	2.4	0.8	2.1	6.3	7.8	13.5	6.1	0.3	0.5	
MWISP G114.142+02.617	-95.3	2.1	0.7	1.7	3.3	8.7	14.3	4.7	0.1	0.4	
MWISP G114.183+02.583	-94.2	2.8	1.3	4.1	6.2	8.5	14.2	6.6	0.6	0.4	
MWISP G114.567+04.567	-79.6	2.5	2.0	5.4	123.0	6.7	12.7	24.3	10.2	0.5	
MWISP G114.642+03.958	-80.8	1.8	1.5	2.8	7.8	6.9	12.8	6.1	0.3	0.5	
MWISP G114.842+04.617	-81.6	5.2	2.9	15.8	110.3	7.0	12.9	24.1	29.3	0.6	HCS01;BKP03
MWISP G114.983+02.200	-94.3	3.2	1.0	3.3	5.3	8.5	14.2	6.1	0.4	0.3	
MWISP G115.058+04.633	-79.4	1.9	2.6	5.2	101.8	6.7	12.7	22.1	8.2	0.5	
MWISP G115.650+03.950	-79.9	2.0	1.0	2.2	21.5	6.8	12.8	10.2	0.7	0.5	BKP03
MWISP G115.833+02.317	-92.8	2.1	1.1	2.5	6.2	8.3	14.1	6.5	0.3	0.3	
MWISP G115.867+03.858	-78.6	2.5	0.5	1.3	8.9	6.6	12.7	6.2	0.2	0.4	
MWISP G115.958+03.917	-80.3	1.6	1.4	2.2	3.2	6.8	12.9	3.6	0.1	0.5	
MWISP G116.108+04.550	-78.2	3.4	1.8	6.2	58.8	6.6	12.7	16.5	5.4	0.5	BKP03
MWISP G116.250+02.542	-91.8	2.4	0.6	1.5	3.0	8.2	14.1	4.2	0.1	0.4	
MWISP G116.400+03.942	-79.7	2.1	0.7	1.7	39.6	6.7	12.8	13.7	1.0	0.5	
MWISP G116.467+03.008	-91.0	2.2	1.1	2.5	9.9	8.1	14.0	8.1	0.5	0.4	
MWISP G116.492+04.008	-79.9	2.6	1.6	4.3	36.6	6.8	12.9	13.4	2.5	0.5	BKP03
MWISP G116.650+03.767	-78.4	1.9	0.6	1.2	16.4	6.6	12.7	8.6	0.3	0.4	
MWISP G116.717+02.892	-90.3	2.5	1.3	3.5	23.5	8.0	13.9	12.6	1.8	0.4	
MWISP G116.892+02.967	-90.4	2.4	1.4	3.5	4.7	8.0	14.0	5.3	0.3	0.4	
MWISP G116.917+03.067	-90.1	3.0	1.3	4.1	5.7	8.0	13.9	5.9	0.5	0.4	
MWISP G116.958+02.967	-89.0	2.5	1.4	3.9	11.2	7.9	13.8	8.4	0.9	0.4	
MWISP G117.250+02.992	-89.5	3.0	2.1	7.0	33.1	7.9	13.9	14.8	4.9	0.4	HCS01;BKP03

Table 1—Continued

Name	V_{LSR} (km s^{-1})	T_{peak} (K)	ΔV (km s^{-1})	I_{CO} ($\text{K} \cdot \text{km s}^{-1}$)	Area (arcmin^2)	d (kpc)	R (kpc)	Size (pc)	Mass ($10^3 M_{\odot}$)	Z Scale (kpc)	Note
(1)	(2)	(3)	(4)	(5)	(6)	(7)	(8)	(9)	(10)	(11)	(12)
MWISP G117.433+01.958	-86.1	2.6	0.8	2.3	34.9	7.5	13.6	14.4	1.5	0.3	
MWISP G117.458+01.858	-89.4	2.5	0.7	1.8	7.3	7.9	13.9	6.7	0.3	0.3	
MWISP G117.492+02.167	-92.7	1.3	0.9	1.4	3.3	8.4	14.3	4.5	0.1	0.3	
MWISP G117.567+02.233	-92.9	1.7	1.2	2.3	3.9	8.4	14.3	5.0	0.2	0.3	
MWISP G117.583+01.750	-90.0	3.6	0.9	3.5	24.5	8.0	14.0	12.8	1.8	0.2	
MWISP G117.733+01.633	-91.8	2.2	2.1	5.1	14.4	8.3	14.2	10.1	1.7	0.2	
MWISP G117.767+01.117	-95.6	8.3	1.4	12.1	29.1	8.8	14.7	15.4	9.2	0.2	HCS01;BKP03
MWISP G117.808+01.583	-96.7	3.4	2.0	7.3	22.7	8.9	14.8	13.7	4.4	0.2	HCS01;BKP03
MWISP G117.808+01.733	-90.8	2.3	0.7	1.7	10.5	8.1	14.1	8.4	0.4	0.2	
MWISP G117.950+01.550	-93.9	2.1	1.4	3.1	2.9	8.5	14.5	4.2	0.2	0.2	
MWISP G117.958+01.417	-94.3	2.8	0.8	2.2	4.3	8.6	14.5	5.4	0.2	0.2	
MWISP G117.967+01.650	-95.2	4.5	2.7	12.4	9.0	8.7	14.6	8.3	2.7	0.3	BKP03
MWISP G118.017+01.567	-96.8	4.1	2.1	9.3	44.1	9.0	14.8	19.5	11.3	0.2	HCS01
MWISP G118.117+01.592	-91.7	4.3	1.6	7.4	105.5	8.3	14.2	27.9	18.5	0.2	HCS01;BKP03
MWISP G118.142+01.900	-88.4	2.0	1.2	2.5	5.8	7.8	13.9	5.8	0.3	0.3	
MWISP G118.192+01.750	-92.3	4.2	1.5	6.3	38.3	8.3	14.3	16.7	5.7	0.3	HCS01;BKP03
MWISP G118.233+01.633	-91.1	2.1	1.0	2.3	11.9	8.2	14.2	9.1	0.6	0.2	
MWISP G118.258+01.983	-87.7	2.4	1.2	2.9	7.0	7.7	13.8	6.4	0.4	0.3	
MWISP G118.267+01.767	-91.2	5.0	1.1	6.1	7.1	8.2	14.2	6.9	0.9	0.3	
MWISP G118.292+01.467	-91.5	1.9	0.8	1.6	6.6	8.2	14.2	6.6	0.2	0.2	
MWISP G118.342+01.392	-95.4	2.1	0.5	1.1	7.5	8.8	14.7	7.6	0.2	0.2	
MWISP G118.408+02.092	-87.8	1.6	1.3	2.1	4.4	7.7	13.8	4.9	0.2	0.3	
MWISP G118.492+01.608	-87.7	2.0	1.2	2.4	3.0	7.7	13.8	3.9	0.1	0.2	
MWISP G118.750+01.867	-93.1	2.6	0.7	1.8	7.3	8.5	14.4	7.2	0.3	0.3	
MWISP G119.008+01.750	-88.1	2.6	1.0	2.7	5.0	7.8	13.9	5.4	0.3	0.2	
MWISP G119.017+01.708	-86.0	3.7	1.5	5.7	18.2	7.5	13.7	10.3	1.9	0.2	BKP03
MWISP G119.133+01.733	-86.1	5.8	1.6	10.0	46.3	7.5	13.7	16.6	8.9	0.2	HCS01;BKP03
MWISP G119.583+02.058	-80.3	2.0	1.0	2.1	9.3	6.8	13.1	6.6	0.3	0.2	
MWISP G119.642+02.017	-83.0	2.9	0.9	2.8	39.8	7.2	13.4	14.8	2.0	0.3	BKP03
MWISP G119.650+01.917	-82.1	3.8	1.1	4.5	24.5	7.1	13.3	11.4	1.9	0.2	HCS01;BKP03
MWISP G119.742+02.183	-81.9	2.4	1.2	3.0	56.0	7.0	13.3	17.1	2.8	0.3	
MWISP G121.017+01.892	-83.0	4.8	1.5	7.6	36.8	7.2	13.5	14.2	4.9	0.2	HCS01
MWISP G121.217+01.950	-83.0	3.1	1.0	3.3	15.2	7.2	13.6	9.0	0.9	0.2	BKP03
MWISP G121.550+01.742	-82.1	2.8	1.0	2.8	4.1	7.1	13.5	4.4	0.2	0.2	
MWISP G122.558+02.117	-85.1	2.3	1.3	3.3	15.3	7.5	13.9	9.4	0.9	0.3	HCS01;BKP03
MWISP G122.617+02.183	-84.5	3.7	1.7	6.5	16.2	7.4	13.8	9.6	1.9	0.3	HCS01;BKP03
MWISP G122.742+02.083	-83.5	5.4	1.4	8.0	13.4	7.3	13.8	8.6	1.9	0.3	BKP03
MWISP G123.000+01.933	-85.0	2.0	1.1	2.3	5.3	7.5	14.0	5.3	0.2	0.3	
MWISP G123.167+01.892	-87.2	2.8	1.5	4.5	24.6	7.8	14.2	12.5	2.3	0.3	
MWISP G123.300+01.867	-87.9	1.8	1.4	2.7	4.5	7.9	14.3	5.1	0.2	0.3	
MWISP G123.433+02.550	-87.1	5.5	1.2	7.1	34.0	7.8	14.2	14.8	5.0	0.3	HCS01;BKP03
MWISP G123.742+02.067	-77.0	1.8	1.4	2.9	5.4	6.5	13.1	4.7	0.2	0.2	HCS01
MWISP G123.850+02.242	-80.8	2.0	2.0	4.2	12.0	7.0	13.6	7.8	0.8	0.3	
MWISP G123.917+02.250	-80.6	2.3	0.9	2.4	13.3	7.0	13.5	8.2	0.5	0.3	BKP03

Table 1—Continued

Name	V_{LSR} (km s^{-1})	T_{peak} (K)	ΔV (km s^{-1})	I_{CO} ($\text{K} \cdot \text{km s}^{-1}$)	Area (arcmin^2)	d (kpc)	R (kpc)	Size (pc)	Mass ($10^3 M_{\odot}$)	Z Scale (kpc)	Note
(1)	(2)	(3)	(4)	(5)	(6)	(7)	(8)	(9)	(10)	(11)	(12)
MWISP G123.967+01.283	-81.0	3.5	0.9	3.4	9.4	7.1	13.6	6.9	0.5	0.2	
MWISP G123.983+02.500	-89.4	6.2	1.1	7.3	14.1	8.2	14.6	9.9	2.3	0.4	BKP03
MWISP G124.100+02.267	-78.5	2.5	1.3	3.7	23.3	6.7	13.3	10.5	1.3	0.3	BKP03
MWISP G124.150+01.917	-77.1	4.2	1.3	5.6	9.8	6.6	13.2	6.6	0.8	0.2	BKP03
MWISP G124.183+01.308	-80.7	3.1	1.2	4.0	3.7	7.0	13.6	4.1	0.2	0.2	
MWISP G124.200+02.042	-75.8	4.0	1.6	6.9	16.4	6.4	13.1	8.4	1.5	0.2	BKP03
MWISP G124.442+01.442	-81.3	2.8	1.0	3.1	3.2	7.1	13.7	3.8	0.1	0.2	
MWISP G124.492+02.183	-77.4	7.0	1.1	8.2	24.9	6.6	13.3	10.7	3.0	0.3	HCS01;BKP03
MWISP G124.517+01.467	-80.8	4.5	1.6	7.9	10.8	7.1	13.6	7.4	1.4	0.2	HCS01;BKP03
MWISP G124.517+02.067	-77.7	2.4	1.5	3.9	21.1	6.7	13.3	10.0	1.2	0.2	HCS01;BKP03
MWISP G124.608+02.250	-84.6	2.4	1.2	2.9	14.0	7.6	14.1	9.1	0.8	0.3	
MWISP G124.617+02.133	-77.8	2.8	0.9	2.9	3.8	6.7	13.3	3.9	0.1	0.2	
MWISP G124.617+02.267	-78.8	1.9	1.7	3.5	13.7	6.8	13.4	8.1	0.7	0.3	BKP03
MWISP G124.633+00.967	-80.2	2.3	0.9	2.1	11.2	7.0	13.6	7.5	0.4	0.1	
MWISP G124.650+02.542	-86.6	10.0	4.5	47.9	616.5	7.8	14.3	63.5	619.7	0.3	BW94;HCS01
MWISP G124.658+00.850	-79.8	2.7	0.9	2.7	11.5	6.9	13.5	7.5	0.5	0.1	
MWISP G124.717+01.783	-76.6	3.0	1.4	4.5	5.5	6.5	13.2	4.7	0.3	0.2	
MWISP G124.867+01.658	-83.5	3.1	0.6	2.0	4.6	7.4	14.0	4.9	0.2	0.2	
MWISP G124.933+02.142	-84.6	2.2	1.7	4.0	10.6	7.6	14.1	7.9	0.8	0.3	BKP03
MWISP G125.042+02.158	-84.8	4.7	1.9	9.1	56.2	7.6	14.2	18.6	10.1	0.3	HCS01;BKP03
MWISP G125.050+01.608	-83.7	4.5	1.2	6.0	60.8	7.5	14.0	19.1	7.0	0.2	HCS01;BKP03
MWISP G125.058+01.108	-87.0	1.7	1.1	1.9	7.3	7.9	14.4	6.7	0.3	0.2	
MWISP G125.100+01.417	-82.4	4.7	1.2	6.0	36.8	7.3	13.9	14.4	4.0	0.2	HCS01;BKP03
MWISP G125.158+01.317	-87.6	1.2	3.3	3.8	10.1	8.0	14.5	8.1	0.8	0.2	
MWISP G125.158+01.550	-82.2	4.3	1.7	7.9	53.0	7.3	13.9	17.3	7.6	0.2	BKP03
MWISP G125.167+01.958	-88.7	3.1	1.4	4.7	56.3	8.2	14.7	20.1	6.1	0.3	HCS01;BKP03
MWISP G125.242+03.167	-85.7	2.5	1.0	2.8	7.4	7.7	14.3	6.6	0.4	0.4	
MWISP G125.317+01.150	-81.0	2.7	1.1	3.0	5.1	7.1	13.8	4.9	0.2	0.1	
MWISP G125.342+01.283	-80.6	2.5	1.1	3.1	9.4	7.1	13.7	6.9	0.5	0.2	
MWISP G125.358+01.233	-79.4	2.4	1.1	2.9	9.5	6.9	13.6	6.8	0.4	0.1	
MWISP G125.508+02.258	-87.9	3.2	1.5	5.3	25.5	8.1	14.6	13.3	3.0	0.3	BKP03
MWISP G125.567+02.750	-89.0	3.5	1.3	4.7	4.1	8.2	14.7	5.0	0.4	0.4	BKP03
MWISP G125.658+02.717	-89.3	2.3	1.3	3.1	7.6	8.3	14.8	7.2	0.5	0.4	
MWISP G125.783+02.083	-88.6	1.8	0.8	1.5	2.5	8.2	14.7	3.7	0.1	0.3	
MWISP G125.808+03.050	-86.0	7.7	2.1	17.6	25.6	7.8	14.4	12.8	9.2	0.4	HCS01;BKP03
MWISP G125.883+02.783	-83.5	2.4	0.8	2.0	3.7	7.5	14.1	4.3	0.1	0.4	
MWISP G126.092+02.292	-78.9	2.4	1.4	3.6	10.4	6.9	13.6	7.1	0.6	0.3	
MWISP G126.208+03.167	-86.0	2.7	0.7	2.0	6.8	7.9	14.4	6.5	0.3	0.4	
MWISP G126.258+01.833	-84.0	2.5	0.9	2.5	5.5	7.6	14.2	5.5	0.2	0.2	
MWISP G126.258+02.017	-81.1	3.5	1.3	4.6	91.3	7.2	13.9	22.5	7.5	0.3	HCS01
MWISP G126.300+01.892	-83.4	2.5	0.9	2.4	6.0	7.5	14.1	5.7	0.3	0.2	
MWISP G126.350+02.283	-78.8	4.4	2.0	9.1	73.5	6.9	13.6	19.3	10.9	0.3	HCS01;BKP03
MWISP G126.517+03.150	-85.1	6.1	1.3	8.6	23.3	7.7	14.4	12.0	4.0	0.4	
MWISP G126.650+03.108	-85.7	3.1	1.5	5.0	19.8	7.8	14.5	11.2	2.0	0.4	HCS01

Table 1—Continued

Name	V_{LSR} (km s ⁻¹)	T_{peak} (K)	ΔV (km s ⁻¹)	I_{CO} (K · km s ⁻¹)	Area (arcmin ²)	d (kpc)	R (kpc)	Size (pc)	Mass (10 ³ M _⊙)	Z Scale (kpc)	Note
(1)	(2)	(3)	(4)	(5)	(6)	(7)	(8)	(9)	(10)	(11)	(12)
MWISP G126.683+01.892	-82.9	2.5	0.7	1.8	5.3	7.5	14.1	5.3	0.2	0.2	
MWISP G126.742+01.833	-84.8	2.5	0.6	1.7	4.2	7.7	14.4	4.8	0.1	0.2	
MWISP G126.767+02.800	-80.0	2.7	1.0	3.0	9.1	7.1	13.8	6.8	0.4	0.3	
MWISP G126.917+02.292	-88.9	2.3	1.0	2.4	18.8	8.4	14.9	11.8	1.1	0.3	
MWISP G127.050+02.158	-84.5	2.8	0.8	2.4	5.1	7.7	14.4	5.4	0.2	0.3	
MWISP G127.067+01.967	-82.0	3.7	1.0	3.9	17.8	7.4	14.1	10.1	1.3	0.3	BKP03
MWISP G127.083+01.992	-82.0	3.8	0.9	3.6	18.3	7.4	14.1	10.2	1.2	0.3	BKP03
MWISP G127.217+01.483	-81.1	3.1	3.4	11.3	57.5	7.3	14.0	18.1	11.8	0.2	HCS01;BKP03
MWISP G127.258+01.200	-76.9	2.1	1.5	3.3	54.2	6.7	13.5	16.1	2.7	0.1	
MWISP G127.350+02.400	-87.8	3.3	1.0	3.6	1.9	8.2	14.9	3.1	0.1	0.3	
MWISP G127.408+03.017	-85.9	3.7	1.1	4.1	16.8	7.9	14.6	10.4	1.4	0.4	
MWISP G127.450+01.517	-81.8	2.1	1.9	4.2	19.9	7.4	14.1	10.7	1.5	0.2	
MWISP G127.467+02.442	-80.9	2.2	0.9	2.0	8.1	7.2	14.0	6.5	0.3	0.3	
MWISP G127.550+01.883	-81.6	6.1	2.7	17.4	105.9	7.4	14.1	24.9	34.6	0.2	HCS01
MWISP G127.633+02.533	-82.1	2.9	1.0	3.2	35.6	7.4	14.1	14.4	2.1	0.3	
MWISP G127.658+01.800	-86.1	3.7	0.9	3.6	68.5	8.0	14.7	21.6	5.4	0.3	BKP03
MWISP G127.667+01.300	-82.0	2.1	0.9	1.9	15.8	7.4	14.2	9.5	0.5	0.2	
MWISP G127.833+02.533	-82.1	3.3	0.9	3.0	55.8	7.4	14.2	18.0	3.1	0.3	BKP03
MWISP G127.967+02.017	-84.7	4.1	1.2	5.5	10.4	7.8	14.5	8.0	1.1	0.3	BKP03
MWISP G127.992+02.292	-85.2	2.8	1.1	3.4	7.3	7.9	14.6	6.7	0.5	0.3	
MWISP G128.000+01.808	-87.2	3.3	1.0	3.3	13.9	8.2	14.9	9.8	1.0	0.3	
MWISP G128.100+01.117	-81.4	2.6	1.5	4.2	34.3	7.4	14.1	14.1	2.7	0.1	
MWISP G128.108+01.917	-86.0	3.7	1.5	5.7	6.5	8.1	14.7	6.5	0.8	0.3	
MWISP G128.117+02.508	-80.4	3.8	1.2	4.9	51.9	7.2	14.0	16.9	4.5	0.3	
MWISP G128.183+01.208	-82.2	2.7	1.3	3.6	11.6	7.5	14.3	8.2	0.8	0.2	
MWISP G128.208+01.967	-83.3	2.6	0.6	1.8	22.1	7.7	14.4	11.7	0.8	0.3	
MWISP G128.583+02.767	-85.2	2.8	0.9	2.7	19.8	8.0	14.7	11.5	1.1	0.4	
MWISP G128.783+02.008	-81.9	11.5	2.9	35.9	327.5	7.5	14.3	44.5	227.9	0.3	BW94;HCS01;BKP03
MWISP G128.792+01.342	-83.0	3.0	2.3	7.3	359.0	7.7	14.4	47.8	53.6	0.2	HCS01
MWISP G128.917+02.142	-80.0	6.2	2.3	15.0	51.6	7.2	14.1	16.9	13.7	0.3	HCS01
MWISP G129.067+01.600	-81.2	2.5	1.3	3.3	34.3	7.4	14.3	14.1	2.1	0.2	BKP03
MWISP G129.100+01.967	-81.2	8.1	1.8	15.4	45.2	7.4	14.2	16.2	13.0	0.3	BW94;HCS01
MWISP G129.167+01.417	-80.3	2.6	1.4	3.8	25.2	7.3	14.2	11.9	1.7	0.2	
MWISP G129.250+01.633	-81.0	2.6	0.8	2.2	13.1	7.4	14.2	8.6	0.5	0.2	BKP03
MWISP G129.342+00.767	-79.0	1.8	1.2	2.3	13.1	7.2	14.0	8.4	0.5	0.1	
MWISP G129.550+01.517	-80.5	4.0	0.9	4.0	58.0	7.4	14.2	18.4	4.3	0.2	HCS01
MWISP G129.567+01.692	-80.1	7.8	1.6	12.9	45.9	7.3	14.2	16.1	10.8	0.2	HCS01;BKP03
MWISP G129.600+01.450	-80.1	2.8	1.1	3.2	7.8	7.3	14.2	6.4	0.4	0.2	
MWISP G129.617+01.542	-81.2	2.8	1.7	4.8	20.3	7.5	14.3	10.9	1.8	0.2	BKP03
MWISP G129.633+01.358	-81.5	2.8	0.7	2.2	17.8	7.5	14.4	10.2	0.7	0.2	
MWISP G129.642+01.433	-81.7	3.0	1.5	4.9	9.3	7.6	14.4	7.4	0.9	0.2	
MWISP G129.808+01.492	-82.9	2.6	0.9	2.4	10.5	7.8	14.6	8.1	0.5	0.2	
MWISP G129.892+01.867	-80.9	2.5	1.2	3.2	38.6	7.5	14.3	15.2	2.4	0.2	
MWISP G130.150+00.983	-79.7	3.1	0.7	2.4	6.2	7.3	14.2	5.7	0.2	0.1	

Table 1—Continued

Name	V_{LSR} (km s^{-1})	T_{peak} (K)	ΔV (km s^{-1})	I_{CO} ($\text{K} \cdot \text{km s}^{-1}$)	Area (arcmin^2)	d (kpc)	R (kpc)	Size (pc)	Mass ($10^3 M_{\odot}$)	Z Scale (kpc)	Note
(1)	(2)	(3)	(4)	(5)	(6)	(7)	(8)	(9)	(10)	(11)	(12)
MWISP G130.367+02.350	-75.9	2.4	1.1	2.8	4.7	6.8	13.7	4.5	0.2	0.3	
MWISP G130.450+01.567	-83.5	4.3	1.0	4.6	12.4	7.9	14.8	8.9	1.2	0.2	BKP03
MWISP G130.517+01.550	-84.3	3.0	1.1	3.5	7.6	8.1	14.9	7.0	0.6	0.2	
MWISP G130.658+01.442	-79.0	5.6	1.6	9.5	98.1	7.3	14.2	23.7	17.0	0.2	HCS01;BKP03
MWISP G130.667+01.617	-87.4	2.5	1.3	3.3	2.8	8.6	15.4	4.2	0.2	0.2	
MWISP G130.767+00.992	-78.8	2.0	1.6	3.7	15.4	7.3	14.2	9.2	1.0	0.1	
MWISP G130.967+02.000	-82.3	2.4	1.0	2.5	26.1	7.8	14.7	12.9	1.3	0.3	
MWISP G131.017+01.242	-78.7	4.2	1.1	4.9	33.9	7.3	14.2	13.8	3.0	0.2	HCS01;BKP03
MWISP G131.167+00.667	-79.9	2.8	0.9	2.8	9.3	7.5	14.4	7.3	0.5	0.1	BKP03
MWISP G131.200+01.117	-77.9	4.8	1.3	6.7	58.9	7.2	14.1	18.0	7.0	0.1	HCS01;BKP03
MWISP G131.450+00.850	-79.5	4.3	0.9	4.4	52.5	7.5	14.4	17.7	4.4	0.1	HCS01;BKP03
MWISP G131.458+02.050	-79.0	2.9	1.0	3.2	17.1	7.4	14.3	9.9	1.0	0.3	BKP03
MWISP G131.467+01.167	-77.0	1.7	2.1	3.9	26.3	7.1	14.1	11.8	1.7	0.1	
MWISP G131.600+02.042	-78.8	3.3	1.4	5.0	23.9	7.3	14.3	11.6	2.1	0.3	
MWISP G131.658+01.817	-78.6	1.7	1.4	2.8	29.3	7.3	14.3	12.8	1.5	0.2	
MWISP G131.742+01.067	-79.3	1.7	1.9	3.3	8.2	7.5	14.4	6.8	0.5	0.1	BKP03
MWISP G131.858+01.342	-78.4	8.7	2.3	21.7	62.3	7.3	14.3	18.8	24.6	0.2	BW94;HCS01
MWISP G132.042+01.158	-78.3	3.2	1.3	4.3	40.9	7.3	14.3	15.2	3.2	0.1	HCS01;BKP03
MWISP G132.158+01.517	-78.3	4.4	1.1	4.9	45.2	7.3	14.3	16.0	4.0	0.2	HCS01
MWISP G132.158+01.650	-78.0	2.7	1.3	3.8	78.7	7.3	14.3	21.2	5.5	0.2	HCS01
MWISP G132.167+02.517	-86.6	4.8	1.0	5.2	35.6	8.7	15.6	16.9	4.7	0.4	HCS01
MWISP G132.292+02.450	-87.7	2.7	1.1	3.1	22.7	8.9	15.8	13.7	1.9	0.4	
MWISP G132.308+01.967	-84.7	4.5	1.5	7.2	43.0	8.4	15.3	18.0	7.4	0.3	BKP03
MWISP G132.392+02.217	-85.6	2.1	1.1	2.4	22.2	8.6	15.5	13.1	1.3	0.3	
MWISP G132.783+02.208	-77.8	3.3	1.3	4.5	16.0	7.3	14.4	9.4	1.3	0.3	BKP03
MWISP G133.192+01.608	-74.2	6.1	0.8	5.1	18.8	6.8	13.9	9.5	1.5	0.2	BKP03
MWISP G133.217+01.683	-74.4	3.0	0.9	2.8	5.6	6.9	14.0	5.1	0.2	0.2	BKP03
MWISP G133.217+01.967	-73.2	2.0	1.7	3.5	24.7	6.7	13.8	10.8	1.3	0.2	BKP03
MWISP G133.242+02.250	-72.4	2.6	1.2	3.3	25.9	6.6	13.7	10.9	1.3	0.3	
MWISP G133.308+02.317	-72.6	2.3	1.0	2.5	21.3	6.6	13.7	9.9	0.8	0.3	
MWISP G133.408+02.050	-74.3	4.2	2.0	8.8	32.0	6.9	14.0	12.7	4.5	0.2	HCS01;BKP03
MWISP G133.500+02.000	-73.9	1.8	1.6	2.9	5.8	6.8	13.9	5.1	0.2	0.2	
MWISP G133.508+02.300	-75.6	2.5	1.5	4.1	4.8	7.1	14.2	4.8	0.3	0.3	
MWISP G133.533+02.067	-74.0	2.9	1.2	3.6	26.2	6.9	14.0	11.4	1.5	0.2	
MWISP G133.558+01.817	-79.6	2.4	0.7	1.7	3.7	7.7	14.8	4.5	0.1	0.2	
MWISP G133.583+00.217	-74.5	2.5	0.9	2.4	3.6	7.0	14.1	4.0	0.1	0.0	
MWISP G133.583+02.250	-72.4	2.3	2.5	6.0	19.0	6.6	13.7	9.3	1.7	0.3	BKP03
MWISP G133.633+02.150	-70.6	2.0	2.0	4.2	24.9	6.4	13.6	10.3	1.4	0.2	
MWISP G133.783+02.458	-75.2	3.8	1.7	6.8	9.8	7.1	14.2	7.1	1.1	0.3	HCS01;BKP03
MWISP G133.808+02.192	-72.7	1.9	1.9	3.8	55.3	6.7	13.8	16.3	3.2	0.3	
MWISP G133.842+01.583	-78.1	4.2	1.3	5.9	8.2	7.5	14.6	6.8	0.9	0.2	BKP03
MWISP G133.867+00.350	-74.1	2.5	0.9	2.4	63.3	6.9	14.1	17.9	2.5	0.0	
MWISP G133.950+02.442	-72.3	2.2	0.8	1.9	23.5	6.6	13.8	10.4	0.7	0.3	
MWISP G134.150+01.992	-76.6	4.8	1.8	9.0	6.3	7.3	14.4	5.7	0.9	0.3	HCS01;BKP03

Table 1—Continued

Name	V_{LSR} (km s^{-1})	T_{peak} (K)	ΔV (km s^{-1})	I_{CO} ($\text{K} \cdot \text{km s}^{-1}$)	Area (arcmin^2)	d (kpc)	R (kpc)	Size (pc)	Mass ($10^3 M_{\odot}$)	Z Scale (kpc)	Note
(1)	(2)	(3)	(4)	(5)	(6)	(7)	(8)	(9)	(10)	(11)	(12)
MWISP G134.483+01.767	-73.2	2.2	0.7	1.6	7.2	6.9	14.0	5.8	0.2	0.2	
MWISP G134.517+01.367	-77.2	2.7	0.5	1.5	6.8	7.5	14.6	6.1	0.2	0.2	
MWISP G134.583+01.783	-73.3	2.6	0.9	2.4	7.8	6.9	14.1	6.1	0.3	0.2	
MWISP G134.700+02.708	-71.7	2.3	1.0	2.5	28.6	6.6	13.8	11.5	1.1	0.3	HCS01
MWISP G134.758+02.658	-71.5	4.9	1.7	8.7	22.3	6.6	13.8	10.1	2.8	0.3	HCS01;BKP03
MWISP G134.842+00.500	-74.8	3.4	0.5	1.9	24.0	7.2	14.3	11.4	0.8	0.1	
MWISP G134.942+02.383	-71.2	3.4	1.6	5.9	62.8	6.6	13.8	17.1	5.5	0.3	HCS01;BKP03
MWISP G135.208+02.717	-72.1	12.4	1.9	24.8	20.5	6.8	14.0	10.0	7.9	0.3	BW94;HCS01;BKP03
MWISP G135.267+02.800	-71.8	11.0	3.8	45.6	27.3	6.7	13.9	11.4	18.9	0.3	BW94;HCS01
MWISP G135.283+01.242	-82.7	2.2	0.7	1.7	3.8	8.6	15.6	5.1	0.1	0.2	
MWISP G135.317+02.692	-78.3	4.3	1.4	6.4	32.3	7.8	14.9	14.4	4.3	0.4	HCS01;BKP03
MWISP G135.367+02.717	-74.0	6.2	1.7	11.3	23.2	7.1	14.3	11.1	4.4	0.3	HCS01;BKP03
MWISP G135.392+02.692	-78.4	2.7	1.5	4.6	13.1	7.8	14.9	9.1	1.2	0.4	HCS01
MWISP G135.542+02.667	-74.3	3.1	1.2	4.1	4.3	7.2	14.3	4.6	0.3	0.3	
MWISP G135.617+02.767	-72.3	9.4	1.7	17.0	15.5	6.8	14.1	8.6	4.0	0.3	HCS01;BKP03
MWISP G135.633+02.992	-72.5	4.2	1.3	5.8	8.2	6.9	14.1	6.2	0.7	0.4	BKP03
MWISP G135.667+02.483	-70.7	3.3	1.3	4.8	17.9	6.6	13.9	9.0	1.2	0.3	BKP03
MWISP G135.667+02.942	-73.0	3.4	1.0	3.8	2.9	7.0	14.2	3.5	0.1	0.4	
MWISP G135.692+03.058	-72.3	4.1	1.0	4.4	3.0	6.9	14.1	3.5	0.2	0.4	
MWISP G135.742+03.100	-72.9	3.0	0.6	1.9	4.0	7.0	14.2	4.2	0.1	0.4	
MWISP G135.833+02.367	-69.8	2.9	2.8	8.5	30.8	6.5	13.8	11.7	3.7	0.3	BKP03
MWISP G135.950+00.800	-76.2	5.2	1.7	9.2	378.8	7.6	14.7	48.5	69.4	0.1	HCS01;BKP03
MWISP G135.992+00.667	-78.4	7.4	1.6	12.4	7.5	8.0	15.1	6.9	1.9	0.1	BKP03
MWISP G136.050+00.733	-71.1	2.9	0.8	2.6	5.7	6.8	14.1	5.0	0.2	0.1	BKP03
MWISP G136.067+00.367	-80.8	2.5	1.4	3.8	81.6	8.4	15.5	24.8	7.5	0.1	
MWISP G136.600+02.950	-72.3	5.1	1.5	7.9	9.9	7.0	14.2	7.0	1.2	0.4	BKP03
MWISP G136.650+02.867	-71.7	4.1	1.2	5.0	17.0	6.9	14.2	9.2	1.3	0.3	HCS01
MWISP G136.717+01.467	-81.3	3.2	1.5	5.2	8.5	8.6	15.8	7.9	1.1	0.2	BKP03
MWISP G136.742+03.042	-70.8	5.1	1.4	7.5	12.9	6.8	14.0	7.8	1.5	0.4	HCS01;BKP03
MWISP G137.517+00.800	-77.7	2.2	1.2	2.6	5.8	8.1	15.3	6.1	0.3	0.1	
MWISP G138.367+02.317	-66.9	2.8	1.1	3.3	6.7	6.4	13.8	5.2	0.3	0.3	
MWISP G138.383+00.833	-74.7	2.5	1.1	3.0	7.9	7.7	15.0	6.9	0.5	0.1	
MWISP G138.417+00.658	-72.8	2.9	1.7	5.1	170.8	7.4	14.7	31.7	16.4	0.1	
MWISP G138.442+02.150	-68.6	3.1	1.1	3.8	7.1	6.7	14.1	5.6	0.4	0.3	BKP03
MWISP G138.567+00.792	-77.0	2.5	1.1	3.0	11.5	8.2	15.5	8.9	0.8	0.1	HCS01;BKP03
MWISP G138.633+00.817	-75.1	3.4	1.7	6.0	6.4	7.9	15.2	6.2	0.7	0.1	
MWISP G138.783+00.417	-76.7	2.5	0.9	2.4	8.8	8.2	15.5	7.7	0.5	0.1	BKP03
MWISP G139.292+00.458	-74.6	1.9	1.0	2.1	3.5	7.9	15.3	4.4	0.1	0.1	
MWISP G139.308+01.067	-73.2	2.1	1.4	3.2	5.7	7.7	15.0	5.7	0.3	0.1	
MWISP G140.800-00.483	-66.2	5.3	1.4	7.6	4.3	6.7	14.2	4.2	0.4	-0.1	
MWISP G140.842+00.550	-58.4	2.0	0.8	1.7	12.6	5.5	13.1	6.2	0.2	0.1	
MWISP G141.000+00.500	-58.3	2.0	0.8	1.6	12.4	5.5	13.1	6.2	0.2	0.0	
MWISP G141.050+00.642	-57.3	3.9	1.9	8.0	60.5	5.4	13.0	13.6	4.8	0.1	
MWISP G141.133+00.758	-57.2	2.5	0.7	2.0	5.8	5.4	13.0	4.0	0.1	0.1	

Table 1—Continued

Name	V_{LSR} (km s^{-1})	T_{peak} (K)	ΔV (km s^{-1})	I_{CO} ($\text{K} \cdot \text{km s}^{-1}$)	Area (arcmin^2)	d (kpc)	R (kpc)	Size (pc)	Mass ($10^3 M_{\odot}$)	Z Scale (kpc)	Note
(1)	(2)	(3)	(4)	(5)	(6)	(7)	(8)	(9)	(10)	(11)	(12)
MWISP G141.133+01.517	-55.5	5.4	2.3	13.0	57.8	5.1	12.7	12.7	6.7	0.1	
MWISP G141.342+02.750	-60.7	2.4	0.9	2.2	9.1	5.9	13.5	5.7	0.2	0.3	
MWISP G141.350+00.642	-57.9	2.2	1.2	2.7	3.8	5.5	13.1	3.2	0.1	0.1	
MWISP G141.492+00.383	-56.7	2.9	1.3	3.9	19.8	5.3	12.9	7.7	0.7	0.0	
MWISP G141.567+02.583	-65.6	2.2	1.1	2.6	4.0	6.8	14.3	4.1	0.1	0.3	
MWISP G141.600+03.533	-57.3	2.7	0.6	1.8	6.7	5.4	13.0	4.4	0.1	0.3	
MWISP G141.617+03.608	-56.7	3.0	0.8	2.5	14.1	5.3	12.9	6.4	0.3	0.3	
MWISP G141.650+02.350	-66.9	1.9	1.9	3.7	12.2	7.0	14.5	7.8	0.7	0.3	
MWISP G141.683+03.542	-55.7	2.7	1.3	3.8	17.6	5.2	12.8	7.0	0.6	0.3	
MWISP G141.992+03.158	-58.1	3.3	0.8	2.6	5.9	5.6	13.2	4.2	0.2	0.3	
MWISP G143.117+00.617	-59.0	3.5	1.2	4.3	7.7	5.9	13.5	5.2	0.4	0.1	
MWISP G143.117+00.633	-59.0	3.4	1.2	4.3	6.5	5.9	13.5	4.7	0.3	0.1	
MWISP G143.117+00.967	-56.5	3.0	1.1	3.4	14.0	5.5	13.2	6.6	0.5	0.1	
MWISP G143.258+00.917	-57.2	1.6	1.7	3.1	15.2	5.7	13.4	7.1	0.5	0.1	
MWISP G143.358+01.583	-51.6	2.5	0.8	2.2	24.7	4.8	12.5	7.8	0.4	0.1	
MWISP G143.500+00.642	-57.8	2.1	1.0	2.2	6.0	5.8	13.5	4.4	0.1	0.1	
MWISP G143.508+00.683	-69.3	2.6	1.9	5.6	13.6	7.9	15.5	9.4	1.6	0.1	New Arm
MWISP G143.508+01.658	-54.3	3.1	2.9	9.9	10.3	5.2	12.9	5.4	0.9	0.2	
MWISP G143.617+01.483	-54.1	3.8	2.6	10.1	124.0	5.2	12.9	19.1	11.8	0.1	
MWISP G143.633+00.792	-56.7	3.6	1.3	4.7	38.3	5.6	13.3	11.4	1.9	0.1	
MWISP G143.667+03.092	-55.3	4.4	1.0	4.8	10.8	5.4	13.1	5.7	0.5	0.3	
MWISP G143.742+00.842	-56.2	5.0	1.4	6.9	22.2	5.6	13.3	8.5	1.6	0.1	
MWISP G143.758-00.208	-62.5	3.8	1.0	4.1	6.1	6.7	14.3	5.2	0.4	0.0	
MWISP G143.767+01.692	-53.6	2.1	1.2	2.7	11.3	5.2	12.9	5.6	0.3	0.2	
MWISP G143.792+00.642	-57.0	1.6	1.9	3.4	18.1	5.7	13.4	7.9	0.7	0.1	
MWISP G143.817+00.767	-57.1	4.1	2.0	8.8	37.1	5.7	13.4	11.4	3.7	0.1	
MWISP G143.833-00.117	-58.6	3.3	1.1	3.8	11.7	6.0	13.7	6.6	0.5	0.0	
MWISP G143.858+00.108	-73.0	4.5	1.0	4.6	5.8	8.9	16.4	6.7	0.7	0.0	New Arm
MWISP G143.917+00.650	-56.4	3.0	0.9	2.9	40.2	5.7	13.4	11.7	1.3	0.1	
MWISP G144.167+00.900	-59.1	2.3	1.2	2.9	6.2	6.2	13.9	4.8	0.2	0.1	
MWISP G144.167+00.900	-59.1	2.4	1.3	3.1	6.5	6.1	13.8	4.9	0.2	0.1	
MWISP G144.192+00.642	-54.3	2.6	0.6	1.6	4.8	5.4	13.1	3.6	0.1	0.1	
MWISP G144.250-00.317	-62.0	4.7	0.9	4.4	31.4	6.7	14.3	12.2	2.1	0.0	
MWISP G144.492+00.683	-68.4	2.3	1.3	3.2	6.9	8.0	15.6	6.6	0.5	0.1	New Arm
MWISP G144.633-00.483	-70.2	2.5	2.0	5.1	21.4	8.5	16.0	12.7	2.7	-0.1	New Arm
MWISP G144.658+02.733	-58.8	3.4	1.6	5.7	46.4	6.2	13.9	13.8	3.5	0.3	
MWISP G145.008+00.150	-70.3	2.1	1.9	4.5	23.9	8.6	16.2	13.6	2.7	0.0	New Arm
MWISP G145.033-00.058	-69.6	2.7	1.1	3.0	25.2	8.5	16.1	13.8	1.8	0.0	New Arm
MWISP G145.100+01.483	-51.7	3.3	1.9	6.7	124.8	5.1	12.9	18.7	7.5	0.1	
MWISP G145.200+02.992	-58.7	10.1	2.5	27.2	153.8	6.3	14.0	25.6	57.1	0.3	BW94
MWISP G145.217-00.217	-68.0	3.8	1.4	5.6	70.8	8.2	15.8	22.5	9.1	0.0	New Arm
MWISP G145.250-00.092	-69.1	2.6	1.6	4.3	17.0	8.5	16.1	11.2	1.7	0.0	New Arm
MWISP G145.317-00.183	-67.9	2.4	1.0	2.6	6.3	8.2	15.8	6.4	0.3	0.0	New Arm
MWISP G145.367-00.033	-71.2	3.6	1.1	4.2	83.3	9.0	16.6	26.9	9.7	0.0	New Arm

Table 1—Continued

Name	V_{LSR} (km s^{-1})	T_{peak} (K)	ΔV (km s^{-1})	I_{CO} ($\text{K} \cdot \text{km s}^{-1}$)	Area (arcmin^2)	d (kpc)	R (kpc)	Size (pc)	Mass ($10^3 M_{\odot}$)	Z Scale (kpc)	Note
(1)	(2)	(3)	(4)	(5)	(6)	(7)	(8)	(9)	(10)	(11)	(12)
MWISP G145.392-00.250	-68.4	2.4	1.3	3.4	32.0	8.3	15.9	15.3	2.6	0.0	New Arm
MWISP G145.458+00.633	-68.4	3.2	2.4	8.0	21.1	8.4	15.9	12.5	4.0	0.1	New Arm
MWISP G145.558+00.433	-68.1	2.2	2.2	5.3	51.9	8.3	15.9	19.5	6.5	0.1	New Arm
MWISP G146.158+00.158	-48.0	4.1	2.2	9.9	3.1	4.7	12.5	2.4	0.2	0.0	
MWISP G146.408+00.517	-50.5	4.2	1.1	5.3	9.3	5.1	12.9	4.9	0.4	0.0	
MWISP G146.517+00.517	-67.9	1.8	0.8	1.6	10.5	8.6	16.2	8.9	0.4	0.1	New Arm
MWISP G146.542-00.067	-64.0	3.2	1.0	3.4	25.9	7.7	15.4	12.7	1.8	0.0	New Arm
MWISP G146.542+00.617	-67.9	2.5	1.6	4.2	9.0	8.6	16.2	8.2	0.9	0.1	New Arm
MWISP G146.817+00.517	-66.3	2.6	0.9	2.3	10.8	8.3	16.0	8.7	0.6	0.1	New Arm
MWISP G146.833+02.267	-60.1	3.6	1.4	5.5	6.2	6.9	14.6	5.4	0.5	0.3	
MWISP G146.942+00.800	-67.7	5.3	1.9	10.9	234.0	8.7	16.3	43.7	66.8	0.1	New Arm
MWISP G146.983+00.042	-64.8	3.4	1.5	5.3	52.5	8.0	15.7	18.9	6.1	0.0	New Arm
MWISP G147.208+00.550	-65.6	2.4	1.3	3.2	10.5	8.3	16.0	8.6	0.8	0.1	New Arm
MWISP G147.292+00.683	-57.5	4.2	0.8	3.8	4.2	6.6	14.3	4.1	0.2	0.1	
MWISP G147.333+01.692	-58.7	3.1	1.7	5.5	3.3	6.8	14.5	3.7	0.2	0.2	
MWISP G147.608+00.808	-64.5	3.0	1.1	3.5	11.2	8.2	15.9	8.8	0.9	0.1	New Arm
MWISP G147.767+01.217	-48.6	7.5	1.6	12.7	53.7	5.0	12.8	12.0	5.9	0.1	
MWISP G147.792+00.458	-65.2	2.0	2.9	6.0	19.5	8.5	16.1	12.1	2.8	0.1	New Arm
MWISP G147.833+00.692	-52.4	2.5	3.4	8.7	4.6	5.7	13.5	3.7	0.4	0.1	
MWISP G147.833+01.058	-47.4	3.9	2.0	8.4	4.5	4.9	12.8	3.1	0.3	0.1	
MWISP G147.833+01.117	-48.8	10.1	1.4	15.1	20.5	5.1	12.9	7.4	2.7	0.1	
MWISP G147.842+00.558	-64.3	2.1	0.9	2.1	12.7	8.2	15.9	9.4	0.6	0.1	New Arm
MWISP G147.883+01.108	-47.3	5.2	1.5	8.3	7.8	4.8	12.7	4.3	0.5	0.1	
MWISP G148.033+00.633	-51.6	4.0	2.0	8.3	4.1	5.6	13.4	3.4	0.3	0.1	
MWISP G148.233+01.433	-66.6	3.4	0.9	3.1	7.4	9.0	16.7	7.7	0.6	0.2	New Arm
MWISP G148.233+02.500	-58.7	1.9	1.6	3.2	9.2	7.0	14.8	6.7	0.5	0.3	
MWISP G148.267-00.108	-53.8	3.7	0.8	3.1	10.3	6.1	13.9	6.2	0.4	0.0	
MWISP G148.317+02.608	-57.6	2.0	2.0	4.3	13.3	6.8	14.6	8.0	0.9	0.3	
MWISP G148.350+01.167	-55.3	3.5	0.9	3.2	5.0	6.4	14.2	4.4	0.2	0.1	
MWISP G148.367+02.442	-57.4	6.2	1.7	10.9	30.4	6.8	14.6	12.2	5.2	0.3	
MWISP G148.383+01.258	-54.7	9.0	1.6	15.2	14.0	6.3	14.1	7.5	2.8	0.1	
MWISP G148.417+00.550	-54.5	2.6	1.0	2.7	2.8	6.3	14.1	3.0	0.1	0.1	
MWISP G148.417+02.608	-57.5	3.0	1.0	3.1	7.7	6.8	14.6	6.0	0.4	0.3	
MWISP G148.433+00.608	-54.3	2.1	1.1	2.6	6.7	6.2	14.0	5.0	0.2	0.1	
MWISP G148.767+00.733	-52.3	3.4	2.1	7.6	9.6	5.9	13.7	5.8	0.8	0.1	
MWISP G148.800+00.667	-52.5	8.0	2.5	20.6	17.3	5.9	13.7	8.0	4.2	0.1	
MWISP G148.850+00.858	-60.4	4.6	2.9	14.0	179.2	7.7	15.4	33.8	51.2	0.1	
MWISP G148.867+00.258	-53.3	5.5	1.5	8.8	53.8	6.1	13.9	14.6	6.0	0.0	
MWISP G148.917+00.567	-52.6	4.9	1.0	5.3	20.4	6.0	13.8	8.8	1.3	0.1	
MWISP G148.983+01.167	-59.0	5.5	1.5	8.7	6.7	7.4	15.2	6.0	1.0	0.2	
MWISP G149.167+00.433	-58.6	4.1	0.8	3.6	18.7	7.4	15.1	10.3	1.2	0.1	

Note. — Column (1): source named by MWISP project and T_{peak} position in Galactic Coordinate. Columns (2)–(5): results of Gaussian fit to the spectra. Column (6): solid angle defined by the 3σ limits. Columns (7)–(8): heliocentric distance and galactocentric radius; both are derived by galactic parameters obtained by Reid et al. (2014). Column (9):

equivalent diameters of the molecular clouds corrected by the beam size of the telescope. Column (10): cloud mass calculated by $X=1.8 \times 10^{20} \text{cm}^{-2} (\text{K} \cdot \text{km s}^{-1})^{-1}$ (Dame et al. 2001). Column (11): scale height ($=D \sin(b)$). Column (12): BW94: sources detected by Brand & Wouterloot (1994); HCS01: sources detected by Heyer et al. (2001); BKP03: sources detected by Brunt et al. (2003); New Arm: clouds supposed to belong to the new spiral arm detected by Sun et al. (2015).